Inorganic Chemistry

Article

Cite This: Inorg. Chem. 2019, 58, 3646−3660

pubs.acs.org/IC

Oligophosphine-thiocyanate Copper(I) and Silver(I) Complexes and Their Borane Derivatives Showing Delayed Fluorescence

Gomathy Chakkaradhari,[†] Toni Eskelinen,[†] Cecilia Degbe,[†,∥] Andrey Belyaev,[†] Alexey S. Melnikov,[‡] Elena V. Grachova,[§] Sergey P. Tunik,[§] Pipsa Hirva,[†] and Igor O. Koshevoy*[,†]

[†]Department of Chemistry, University of Eastern Finland, 80101 Joensuu, Finland

[‡]Peter the Great St. Petersburg Polytechnic University, Polytechnicheskaya, 29, 195251 St. Petersburg, Russia

[§]Institute of Chemistry, St. Petersburg State University, Universitetskiy pr. 26, Petergof, 198504 St. Petersburg, Russia

Supporting Information

ABSTRACT: The series of chelating phosphine ligands, which contain bidentate $\mathbf{P^2}$ (bis[(2-diphenylphosphino)-phenyl] ether, DPEphos; 4,5-bis(diphenylphosphino)-9,9-dimethylxanthene, Xantphos; 1,2-bis(diphenylphosphino)-benzene, dppb), tridentate $\mathbf{P^3}$ (bis(2-diphenylphosphinophenyl)phenylphosphine), and tetradentate $\mathbf{P^4}$ (tris(2-diphenylphosphino)phenylphosphine) ligands, was used for the preparation of the corresponding dinuclear $[M(\mu_2\text{-SCN})\mathbf{P^2}]_2$ (M = Cu, **1**, **3**, **5**; M = Ag, **2**, **4**, **6**) and mononuclear $[CuNCS(\mathbf{P^3}/\mathbf{P^4})]$ (**7**, **9**) and $[AgSCN(\mathbf{P^3}/\mathbf{P^4})]$ (**8**, **10**) complexes. The reactions of $\mathbf{P^4}$ with silver salts in a 1:2 molar ratio produce tetranuclear clusters $[Ag_2(\mu_3\text{-SCN})(t\text{-SCN})(\mathbf{P^4})]_2$ (**11**) and $[Ag_2(\mu_3\text{-SCN})(\mathbf{P^4})]_2^{2+}$ (**12**). Complexes **7**−**11** bearing terminally coordinated SCN ligands were efficiently converted into derivatives **13**−**17** with the weakly coordinating $^{-}SCN{:}B(C_6F_5)_3$ isothiocyanatoborate ligand. Compounds **1** and **5**−**17** exhibit thermally activated delayed fluorescence (TADF) behavior in the solid state. The excited states of thiocyanate species are dominated by the ligand to ligand SCN → π(phosphine) charge transfer transitions mixed with a variable contribution of MLCT. The boronation of SCN groups changes the nature of both the S_1 and T_1 states to (L + M)LCT d,p(M, P) → π(phosphine). The localization of the excited states on the aromatic systems of the phosphine ligands determines a wide range of luminescence energies achieved for the title complexes (λ_{em} varies from 448 nm for **1** to 630 nm for **10c**). The emission of compounds **10** and **15**, based on the $\mathbf{P^4}$ ligand, strongly depends on the solid-state packing (λ_{em} = 505 and 625 nm for two crystalline forms of **15**), which affects structural reorganizations accompanying the formation of electronically excited states.

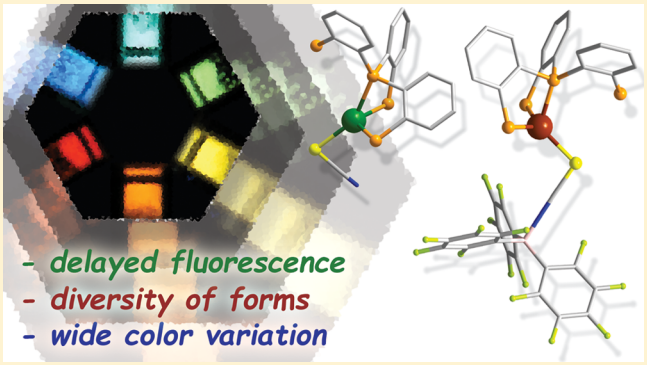

INTRODUCTION

The chemistry of luminescent copper(I) complexes has been significantly revitalized by the phenomenon of thermally activated delayed fluorescence (TADF), which was found to be an intrinsic molecular property of a gradually increasing number of these compounds.[1−5] The given photophysical mechanism implies a small energy gap between the lowest lying singlet and triplet excited states ($\Delta E(S_1-T_1)$ is preferably less than 1000 cm^{-1}) that makes possible the fast population of the T_1 state (via $S_1 \rightarrow T_1$ intersystem crossing, ISC) and its efficient thermal equilibration with emissive S_1 state by means of reverse ISC ($T_1 \rightarrow S_1$). This excited state dynamics, which involves both S_1 and T_1 states, can result in relatively short-lived (τ_{obs} of a few microseconds) and intense photoemission even in the case of a moderate spin−orbit coupling (SCO) induced by a d^{10} copper ion. Therefore, Cu(I) TADF luminophores are considered as a promising and affordable alternative to phosphorescent complexes of noble metals, particularly in view of their application as dopant emitters for efficient electroluminescent devices.[6−12]

The prevailing charge transfer character of the lowest excited states of copper(I) species, which exhibit delayed fluorescence (e.g., metal to ligand charge transfer, MLCT), provides a sufficient spatial separation between the unpaired electrons (i.e., small overlap between the highest occupied and lowest unoccupied molecular orbitals) and thus ensures the required small magnitude of $\Delta E(S_1-T_1)$ splitting. Consequently, modulation of the photophysical properties of Cu(I) TADF emitters is typically achieved by varying the electronic characteristics of the ligand contributing to LUMO that primarily affects the energy of the excited state. This approach, however, puts certain synthetic constraints on the tuning of the luminescence color of Cu(I) complexes, which rarely demonstrate a wide variation of the emission wavelengths.[13−19]

Received: November 11, 2018
Published: February 22, 2019

DOI: 10.1021/acs.inorgchem.8b03166
Inorg. Chem. 2019, 58, 3646−3660

Changing the copper for silver ion, which frequently adopts a similar ligand environment, is a convenient option to influence the electronic structure and the luminescence behavior of target complexes. In comparison to Cu(I), the energetically lower lying d orbitals of Ag(I) lead to a larger energy gap and therefore cause a hypsochromic shift of absorption and emission bands. On the other hand, greater stabilization of silver d electrons and as a result higher oxidation potential of Ag(I) often diminish the metal contribution to frontier molecular orbitals that greatly decreases the probability of MLCT electronic transitions. Thus, Ag(I) luminophores are less prone to exhibiting the delayed fluorescence relative to their Cu(I) congeners.[20−24] This issue might be resolved by utilizing the electron-rich ancillary ligands, which raise the energy of d orbitals and/or substantially contribute to the HOMO, thus facilitating charge transfer transitions (MLCT or LLCT/XLCT and their mixture) and promoting fast and efficient TADF.[20,21,23]

In this work we attempted to address the question of altering the solid-state photophysical performance of a series of copper(I) and silver(I) complexes by employing readily accessible di-, tri-, and tetradentate phosphine ligands, which are expected to play a major role in the excited state. The variable amount of P-donor functions has an essential impact on the energies of the radiative electronic transitions, which are also strongly affected by the crystal packing. The bidentate nature of the auxiliary thiocyanate anions not only allowed the construction of di- and tetranuclear compounds, but also can be used for generating the electronically different $^{-}$SCN:B-$(C_6F_5)_3$ ligand, which has not been exploited previously in the coordination chemistry of transition metals.

EXPERIMENTAL SECTION

General Comments. The ligands bis(2-diphenylphosphinophenyl)phenylphosphine (**P^3**) and tris(2-diphenylphosphino)phenylphosphine (**P^4**), were prepared according to the reported procedures.[25,26] Tetrahydrofuran (THF) was distilled over Na-benzophenone ketyl under a nitrogen atmosphere prior to use. Other reagents were used as received. The solution ^{1}H, ^{31}P{^{1}H} NMR and ^{1}H−^{1}H COSY spectra were recorded on Bruker 400 MHz Avance and AMX 400 spectrometers. Microanalyses were carried out at the analytical laboratory of the University of Eastern Finland.

[Cu(μ_2,κ^2-SCN)DPEphos]$_2$ ***(1)***. DPEphos (100 mg, 0.186 mmol) and CuSCN (22.6 mg, 0.185 mmol) were mixed in a dichloromethane/methanol (15 mL, 3:1 v/v mixture) under a nitrogen atmosphere, and the suspension was refluxed for 12 h. The resulting pale solid was removed by filtration. The solvents were evaporated, and the residue was washed with diethyl ether (2 × 5 mL) and recrystallized by slow evaporation of its dichloromethane/acetonitrile (2:1 v/v mixture) solution at room temperature to give colorless crystalline material (70 mg, 58%). IR (KBr; ν(C≡N), cm^{-1}): 2098. ^{31}P{^{1}H} NMR (DMSO-d_6; 298 K; δ): −19.6 (s, br). ^{1}H NMR (CD_3CN, 298 K; δ): 7.35−7.45 (m, 40H, Ph), 7.27 (ddd, 4H J_{HH} ca. 7.8, 1.4 Hz, C_6H_4), 6.97 (dd, 4H, J_{HH} ca. 7.5 Hz, C_6H_4), 6.93 (dm, 4H, J_{HH} 7.5 Hz, C_6H_4), 6.70 (m, 4H, C_6H_4). Anal. Calcd for $C_{74}H_{56}Cu_2N_2O_2P_4S_2$: C, 67.31; H, 4.27; N, 2.12; S, 4.85. Found: C, 67.47; H, 4.48; N, 2.35; S, 4.85.

[Ag(μ_2,κ^1-SCN)DPEphos]$_2$ ***(2)***. DPEphos (70 mg, 0.130 mmol) and AgSCN (21.4 mg, 0.129 mmol) were mixed in dichloromethane (10 mL) under a nitrogen atmosphere, and the suspension was refluxed for 3 h. The solvent was evaporated, and the pale residue was washed with diethyl ether (2 × 5 mL) and recrystallized by slow evaporation of its dichloromethane/hexane (2:1 v/v mixture) solution at +5 °C to give a colorless crystalline material (72 mg, 81%). IR (KBr; ν(C≡N); cm^{-1}): 2091. ^{31}P{^{1}H} NMR (CD_2Cl_2; 298 K; δ): −8.9 (br d, J_{PAg} 366 Hz). ^{1}H NMR (CD_2Cl_2; 298 K; δ): 7.39−7.51 (m, 40H, Ph), 7.25 (d, 4H, J_{HH} ca. 7.5 Hz, C_6H_4), 7.02 (dd, 4H, J_{HH} 7.0 and 7.5 Hz Hz), 6.81−6.86 (m, 8H, C_6H_4). Anal. Calcd for $C_{75}H_{58}Ag_2N_2O_2P_4S_2Cl_2$: C, 60.29; H, 3.91; N, 1.87; S, 4.29. Found: C, 59.91; H, 4.29; N, 1.91; S, 3.98.

[Cu(μ_2,κ^2-SCN)Xantphos]$_2$ ***(3)***. This compound was prepared similarly to **1** using Xantphos (50 mg, 0.086 mmol) and CuSCN (10.5 mg, 0.086 mmol). It was recrystallized by slow evaporation of its dichloromethane/acetonitrile/methanol (1:1:1 v/v/v mixture) solution at room temperature to give a colorless crystalline material (45 mg, 79%). IR (KBr; ν(C≡N); cm^{-1}): 2091. ^{31}P{^{1}H} NMR (DMSO-d_6; 298 K; δ): −19.1 (s, br). ^{1}H NMR (DMSO-d_6; 298 K; δ): 7.67 (dd, 4H, J_{HH} 7.9, 1.3 Hz, xanth-C_6H_3), 7.29−7.44 (m, 40H, Ph), 7.20 (dd, 4H, J_{HH} ca. 7.9 Hz, xanth-C_6H_3), 6.64 (m, 4H, xanth-C_6H_3), 1.64 (s, 12H, CH_3). Anal. Calcd for $C_{80}H_{64}Cu_2N_2O_2P_4S_2$: C, 68.61; H, 4.61; N, 2.00; S, 4.58. Found: C, 68.33; H, 4.66; N, 2.37; S, 4.41.

[Ag(μ_2,κ^2-SCN)Xantphos]$_2$ ***(4)***. This compound was prepared similarly to **2** using Xantphos (70 mg, 0.121 mmol) and AgSCN (20 mg, 0.120 mmol). It was recrystallized by slow evaporation of its dichloromethane/acetonitrile/methanol (2:1:1 v/v/v mixture) solution at +5 °C to give a colorless crystalline material (76 mg, 84%). IR (KBr; ν(C≡N); cm^{-1}): 2088. ^{31}P{^{1}H} NMR (CD_3CN, 298 K; δ): −5.7 (d, J_{PAg} 374 Hz, 4P). ^{1}H NMR (CD_3CN, 298 K; δ): 7.64 (dd, 4H, J_{HH} 7.8, 1.3 Hz, xanth-C_6H_3), 7.26−7.40 (m, 40H, Ph), 7.17 (t, 4H, J_{HH} ca. 7.9 Hz, xanth-C_6H_3), 6.67 (m, 4H, xanth-C_6H_3), 1.69 (s, 12H, CH_3). Anal. Calcd for $C_{80}H_{64}Ag_2N_2O_2P_4S_2$: C, 64.52; H, 4.32; N, 1.88; S, 4.31. Found: C, 64.19; H, 4.52; N, 2.23; S, 3.97.

[Cu(μ_2,κ^2-SCN)dppb]$_2$ ***(5)***. This compound was prepared similarly to **1** using 1,2-bis(diphenylphosphino)benzene, dppb (80 mg, 0.179 mmol), and CuSCN (21.5 mg, 0.176 mmol). It was recrystallized by slow evaporation of its dichloromethane solution at room temperature to give a pale yellow crystalline material (55 mg, 54%). IR (KBr; ν(C≡N); cm^{-1}): 2108. Due to the poor solubility and the dynamic processes in solution, the interpretable NMR spectra could not be acquired. Anal. Calcd for $C_{62}H_{48}Cu_2N_2P_4S_2$: C, 65.54; H, 4.26; N, 2.47; S, 5.64. Found: C, 65.54; H, 4.39; N, 2.55; S, 5.61.

[Ag(μ_2,κ^2-SCN)dppb]$_2$ ***(6)***. This compound was prepared similarly to **2** using dppb (50 mg, 0.112 mmol) and AgSCN (18.4 mg, 0.111 mmol). It was recrystallized by gas phase diffusion of diethyl ether into a dichloromethane solution of **6** at room temperature to give colorless crystalline material (60 mg, 88%). IR (KBr; ν(C≡N); cm^{-1}): 2094. ^{31}P{^{1}H} NMR (CD_3CN, 298 K; δ): 0.5 (m, br). ^{1}H NMR (CD_3CN, 298 K; δ): 7.56 (br s, 4H, C_6H_4), 7.36 (m, 4H, C_6H_4), 7.18 (m, 40H). Anal. Calcd for $C_{62}H_{48}Ag_2N_2P_4S_2$: C, 60.79; H, 3.95; N, 2.29; S, 5.24. Found: C, 60.98; H, 4.33; N, 2.28; S, 4.85.

[CuNCS(P^3)] ***(7)***. **P^3** (60 mg, 0.095 mmol) and CuSCN (11.5 mg, 0.094 mmol) were stirred in dichloromethane (10 mL) for 3 h at room temperature to give a clear pale greenish solution. The reaction mixture was evaporated, and the greenish solid was washed with diethyl ether (2 × 5 mL) and recrystallized by gas phase diffusion of diethyl ether into a dichloromethane solution of **7** at room temperature to give a greenish wire-like crystalline material (60 mg, 85%). IR (KBr; ν(C≡N); cm^{-1}): 2080. ^{31}P{^{1}H} NMR (CD_2Cl_2; 298 K; δ): −1.1 (d br, J_{PP} ca. 140 Hz, 2P), −8.8 (t br, J_{PP} ca. 140 Hz, 1P). ^{1}H NMR (CD_2Cl_2; 298 K; δ): 7.77 (m, 4H, ortho-H, PPh_2), 7.72 (dd, 2H, J_{HH} ca. 7.5 Hz, C_6H_4), 7.51 (dd, 2H, J_{HH} ca. 7.5 Hz, C_6H_4), 7.45 (dd, 4H, meta-H, PPh_2), 7.42 (dd, 2H, J_{HH} ca. 7.5 Hz, meta-H, C_6H_4), 7.37 (m, 1H, para-H, PPh), 7.31 (m, 2H, para-H, PPh_2), 7.31 (m, 2H, ortho-H, C_6H_4), 7.30 (m, 2H, ortho-H, PPh), 7.28 (m, 2H, J_{HH} 7.5 Hz, para-H, PPh_2), 7.19 (m, 2H, meta-H, PPh), 7.09 (t, 4H, J_{HH} ca. 7.5 Hz, meta-H, PPh_2), 6.64 (m, 4H, ortho-H, PPh_2). Anal. Calcd for $C_{43}H_{33}CuNP_3S{\cdot}CH_2Cl_2$: C, 63.12; H, 4.21; N, 1.67; S, 3.83. Found: C, 63.15; H, 4.32; N, 1.85; S, 3.91.

[AgSCN(P^3)] ***(8)***. This compound was prepared similarly to **7** using **P^3** (60 mg, 0.095 mmol) and AgSCN (15.5 mg, 0.093 mmol). It was recrystallized by gas phase diffusion of diethyl ether into a dichloromethane/acetonitrile (2:1 v/v mixture) solution of **8** at room temperature to give greenish crystals (60 mg, 79%). IR (KBr; ν(C≡N); cm^{-1}): 2097. ^{31}P{^{1}H} NMR (acetone-d_6, 298 K, δ): −9.5 (dd br, J_{PP} ca. 195 Hz, J_{AgP} ca. 206 Hz, 2P), −25.25 (t br, J_{PP} ca. 195 Hz, 1P). ^{1}H NMR (acetone-d_6, 298 K, δ): 7.59 (m, 4H, ortho-H,

DOI: 10.1021/acs.inorgchem.8b03166
Inorg. Chem. 2019, 58, 3646−3660

PPh_2), 7.51 (m, 2H, C_6H_4), 7.49 (m, 2H, C_6H_4), 7.41 (m, 2H, C_6H_4), 7.39 (m, 6H, meta + para-H, PPh_2), 7.36 (m, 3H, para-H, PPh_2, and para-H, Ph), 7.29 (dd, 6H, J_{HH} 7.5 and 7.2 Hz, meta-H, PPh_2, and ortho-H, Ph), 7.21 (dd, 1H, meta-H, Ph), 7.12 (m, 2H, C_6H_4), 7.00 (m, 4H, ortho-H, PPh_2). Anal. Calcd for $C_{43}H_{33}AgNP_3S$: C, 64.83; H, 4.17; N, 1.75; S, 4.02. Found: C, 64.88; H, 4.25; N, 1.78; S, 4.05.

*[CuNCS(P^4)] (**9**).* This compound was prepared similarly to **7** using P^4 (71 mg, 0.087 mmol) and CuSCN (10.5 mg, 0.086 mmol). It was recrystallized by gas phase diffusion of diethyl ether into a dichloromethane solution of **9** at room temperature to give a greenish crystalline material (65 mg, 79%). The orange solvent-free form of **9a** was obtained upon gas phase diffusion of pentane into a tetrahydrofuran solution of **9**. IR (KBr; ν(C≡N); cm^{-1}): 2083. $^{31}P\{^1H\}$ NMR (CD_2Cl_2; 193 K; δ): 2.3 (s br, 1P, PPh_2), −3.9 (s br, 1P, PPh_2), −5.78 (m, 1P, $\underline{P}(C_6H_4PPh_2)_3$), −21.7 (s br, 1P, noncoordinated PPh_2). ^1H NMR (CD_2Cl_2; 193 K; δ): 6.1−8.2 (br unresolved m). Anal. Calcd for $C_{55}H_{42}CuNP_4S{\cdot}C_4H_{10}O$: C, 70.12; H, 5.18; N, 1.38; S, 3.17. Found: C, 69.82; H, 5.13; N, 1.40; S, 3.39.

*[AgSCN(P^4)] (**10**).* This compound was prepared similarly to **7** using P^4 (80 mg, 0.098 mmol) and AgSCN (12 mg, 0.072 mmol). It was recrystallized by slow evaporation of a dichloromethane/acetonitrile solution of **10** at room temperature to give pale green block crystals of isomer **10n** (50 mg, 71%). Yellow block crystals of tetrahydrofuran solvates **10b** are formed by gas phase diffusion of pentane into a tetrahydrofuran solution of crude **10** at +5 °C. Bright yellow-orange long crystals of methanol solvate **10c** were obtained by slow evaporation of a dichloromethane/methanol solution of **10** at room temperature. IR (KBr; ν(C≡N); cm^{-1}): 2092. $^{31}P\{^1H\}$ NMR (CD_2Cl_2; 193 K; δ): AB_3 spin system, −11.4 ($^3J_{PP}$ 192 Hz, $^1J_{107AgP}$ 179 Hz, $^1J_{109AgP}$ 203 Hz, 3P), −30.5 ($^3J_{PP}$ 192 Hz, $^1J_{107AgP}$ 112 Hz, $^1J_{109Ag-P}$ 129 Hz, 1P). ^1H NMR (CD_2Cl_2; 193 K; δ): 7.45−7.34 (m, 9H), 7.26−6.90 (unresolved m, 33H). Anal. Calcd for $C_{55}H_{42}AgNP_4S$: C, 67.35; H, 4.31; N, 1.42; S, 3.26. Found: C, 67.35; H, 4.36; N, 1.54; S, 3.01.

*[$Ag_2(\mu_3,\kappa^2$-SCN)(t-SCN)(P^4)]$_2$ (**11**).* This compound was prepared similarly to **7** using P^4 (60 mg, 0.074 mmol) and AgSCN (24 mg, 0.145 mmol). It was recrystallized by gas phase diffusion of diethyl ether into a dichloromethane solution of **11** to give colorless crystals (70 mg, 84%). IR (KBr; ν(C≡N); cm^{-1}): 2121, 2092, 2083. $^{31}P\{^1H\}$ NMR (CD_2Cl_2; 298 K; δ): −4.0 (m br, 3P, PPh_2), −35.9 (m, 1P, $\underline{P}(C_6H_4PPh_2)_3$). ^1H NMR (CD_2Cl_2; 298 K; δ): 7.52 (br unresolved m, 18H), 7.38 (br unresolved m, 12H), 7.28−7.09 (m, 36H), 7.04 (m, 12H), 6.87 (br unresolved m, 6H). Anal. Calcd for $C_{112}H_{84}Ag_4N_4P_8S_4{\cdot}CH_2Cl_2$: C, 57.07; H, 3.65; N, 2.36; S, 5.39. Found: C, 57.14; H, 3.92; N, 2.41; S, 5.55.

*[$Ag_2(\mu_3,\kappa^2$-SCN)(P^4)]$_2(CF_3SO_3)_2$ (**12**).* This compound was prepared similarly to **7** using P^4 (60 mg, 0.074 mmol), AgSCN (12 mg, 0.072 mmol), and $AgCF_3SO_3$ (19 mg, 0.074). It was recrystallized by gas phase diffusion of diethyl ether into a dichloromethane solution of **12** to give colorless crystals (78 mg, 86%). IR (KBr; ν(C≡N); cm^{-1}): 2125, 2094, 2072. $^{31}P\{^1H\}$ NMR (CD_2Cl_2; 298 K; δ): −2.0 (m, 6P, PPh_2), −34.9 (m, 2P, $\underline{P}(C_6H_4PPh_2)_3$). ^1H NMR (CD_2Cl_2; 298 K; δ): 7.48−7.52 (m, 18H), 7.22−7.28 (m, 24H), 7.07−7.18 (m, 30H), 7.03 (m, 6H), 6.80 (m, 6H). Anal. Calcd for $C_{112}H_{84}Ag_4F_6N_2O_6P_8S_4$: C, 54.34; H, 3.42; N, 1.13; S, 5.18. Found: C, 54.19; H, 3.61; N, 1.14; S, 5.23.

*[Cu{SCNB(C_6F_5)$_3$}(P^3)] (**13**).* $B(C_6F_5)_3$ (85 mg, 0.166 mmol) was added under nitrogen to a degassed solution of complex **7** (125 mg, 0.166 mmol) in freshly distilled THF (10 mL). The clear reaction mixture was stirred for 10 h at room temperature, and then it was evaporated; the residue was washed with hexanes (2 × 5 mL). The resulting green solid was recrystallized by gas phase diffusion of pentane into its tetrahydrofuran solution to give a greenish crystalline material (150 mg, 71%). IR (KBr; ν(C≡N); cm^{-1}): 2185. $^{31}P\{^1H\}$ NMR (CD_2Cl_2; 298 K; δ): 1.40 (br d, 2P, $^3J_{PP}$ 131 Hz), −3.40 (br t, 1P, $^3J_{PP}$ 131 Hz). ^{19}F NMR (CD_2Cl_2; 298 K; δ): −165.4 (ddd, 6F, J_{FF} 23.2, 21.9, 7.9 Hz), −160.0 (t, 3F, J_{FF} 21.9 Hz), −134.7 (dd, 6F, J_{FF} 23.2, 21.9, 7.9 Hz). ^1H NMR (CD_2Cl_2; 298 K; δ): 7.70 (m, 2H, C_6H_4), 7.59 (m, 4H, ortho-H Ph), 7.54 (dd, 2H, J_{HH} ca. 7.1 Hz, C_6H_4), 7.44 (dd, 2H, J_{HH} ca. 7.1 Hz, C_6H_4), 7.42−7.24 (m, 13H), 7.18 (dd, 2H), 7.08 (dd, 4H, J_{HH} ca. 7.0 Hz, meta-H Ph), 6.80 (m, 4H, ortho-H Ph). Anal. Calcd for $C_{61}H_{33}BCuF_{15}NP_3S$: C, 57.95; H, 2.63; N, 1.11. Found: C, 58.01; H, 2.65; N, 1.18.

Recrystallization of **13** (50 mg) by gas phase diffusion of diethyl ether into an acetone solution of **13** produced pale yellow crystals of [Cu{SCNB(C_6F_5)$_3$}(P^3S)] (**13S**) (20 mg, 78%). IR (KBr; ν(C≡N); cm^{-1}): 2185. $^{31}P\{^1H\}$ NMR (CD_2Cl_2; 298 K; δ): 39.1 (dd, 1P, J_{PP} 60.5, 6.8 Hz), −10.9 (br m, 1P), −21.7 (br m, 1P). ^1H NMR (CD_2Cl_2; 298 K; δ): 7.63−7.48 (m, 6H), 7.48−7.30 (m, 10H), 7.27 (m, 2H), 7.23−7.04 (m, 10H), 7.03−6.94 (m, 4H), 6.86 (m, 1H). Anal. Calcd for $C_{61}H_{33}BCuF_{15}NP_3S_2$: C, 57.93; H, 3.31; N, 1.01. Found: C, 57.16; H, 3.04; N, 1.16.

*(P^3)AgSCNB(C_6F_5)$_3$ (**14**).* This compound was prepared similarly to **13** using complex **8** (102 mg, 0.128 mmol) and $B(C_6F_5)_3$ (65 mg, 0.127 mmol). It was recrystallized by gas phase diffusion of pentane into a tetrahydrofuran solution of **14** to give a colorless crystalline material (140 mg, 83%). IR (KBr; ν(C≡N); cm^{-1}): 2184. $^{31}P\{^1H\}$ NMR (CD_2Cl_2; 298 K; δ): AB_2 spin system, −4.7 ($^3J_{PP}$ 204 Hz, $^1J_{107AgP}$ 286 Hz, $^1J_{109AgP}$ 330 Hz, 2P), −30.5 ($^3J_{PP}$ 204 Hz, $^1J_{107AgP}$ 129 Hz, $^1J_{109AgP}$ 147 Hz, 1P). ^{19}F NMR (CD_2Cl_2; 298 K; δ): −165.4 (ddd, 6F, J_{FF} 23.3, 21.2, 8.0 Hz), −159.9 (t, 3F, J_{F-F} 21.2 Hz), −134.8 (dd, 6F, J_{FF} 23.3, 8.0 Hz). ^1H NMR (CD_2Cl_2; 298 K; δ): 7.45−7.14 (m, 25H), 7.07−6.96 (m, 8H). Anal. Calcd for $C_{61}H_{33}AgBF_{15}NP_3S{\cdot}C_4H_8O$: C, 56.55; H, 2.99; N, 1.01. Found: C, 56.78; H, 2.89; N, 1.14.

*[(P^4)CuSCNB(C_6F_5)$_3$] (**15**).* This compound was prepared similarly to **13** using complex **9** (190 mg, 0.203 mmol) and $B(C_6F_5)_3$ (103 mg, 0.203 mmol). Hexane (10 mL) was added to the obtained solid residue, and the suspension was ultrasonicated for 3 h at room temperature to give **15** as a pale yellow precipitate (270 mg, 91%), which was recrystallized by gas phase diffusion of pentane into its tetrahydrofuran/diethyl ether solution to give pale green crystals of the tetrahydrofuran solvate form. Slow evaporation of a dichloromethane/hexane (1:1 v/v mixture) solution of **15** at room temperature gave yellow crystals of solvent-free modification **15a**. IR (KBr; ν(C≡N); cm^{-1}): 2183, 2154. $^{31}P\{^1H\}$ NMR (CD_2Cl_2; 298 K; δ): 9.4 (br s). ^{19}F NMR (CD_2Cl_2; 298 K; δ): −166.1 (ddd, 6F, J_{FF} 23.1, 21.0, 7.6 Hz), −161.1 (t, 3F, J_{FF} 21.0 Hz), −134.9 (dd, J_{FF} 23.1, 7.6 Hz). ^1H NMR (CD_2Cl_2; 298 K; δ): 8.24 (br d, 3H, J_{HH} 8.4 Hz, C_6H_4), 7.63 (dd, 3H, J_{HH} ca. 8.4 Hz, C_6H_4), 7.53 (dd, 3H, J_{HH} ca. 8.4 Hz, C_6H_4), 7.28 (m, 3H, J_{HH} 8.4 Hz, C_6H_4), 7.26 (t, 6H, J_{HH} 7.3 Hz, para-H Ph), 7.07 (dd, 12H, J_{HH} ca. 7.3 Hz, meta-H Ph), 6.95 (br unresolved m, 12H, ortho-H Ph). Anal. Calcd for $C_{73}H_{42}BCuF_{15}NP_4S$: C, 60.53; H, 2.92; N, 0.96. Found: C, 60.68; H, 2.96; N, 1.04.

*[(P^4)AgSCNB(C_6F_5)$_3$] (**16**).* This compound was prepared similarly to **13** using complex **10** (165 mg, 0.168 mmol) and $B(C_6F_5)_3$ (86 mg, 0.168 mmol). It was recrystallized by gas phase diffusion of pentane into a tetrahydrofuran solution of **16** at +5 °C to give yellow crystals (210 mg, 83%). IR (KBr; ν(C≡N); cm^{-1}): 2183. $^{31}P\{^1H\}$ NMR (CD_2Cl_2; 298 K; δ): AB_3 spin system, −10.3 ($^3J_{PP}$ 202 Hz, $^1J_{107AgP}$ 200 Hz, $^1J_{109AgP}$ 228 Hz, 3P), −34.3 ($^3J_{PP}$ 202 Hz, $^1J_{107AgP}$ 110 Hz, $^1J_{109AgP}$ 130 Hz, 1P). ^{19}F NMR (CD_2Cl_2; 298 K; δ): −165.6 (ddd, 6F, J_{FF} 23.3, 21.7, 7.9 Hz), −160.3 (t, 3F, J_{FF} 21.7 Hz), −134.8 (dd, 6F, J_{FF} 23.3, 7.9 Hz). ^1H NMR (CD_2Cl_2; 298 K; δ): 7.29 (m, 6H, Ph), 7.25−7.08 (m, 30H, Ph + C_6H_4), 7.03 (m, 3H, C_6H_4), 6.97 (m, 3H, C_6H_4). Anal. Calcd for $C_{73}H_{42}AgBF_{15}NP_4S$: C, 58.74; H, 2.84; N, 0.94; S, 2.15. Found: C, 58.74; H, 2.88; N, 1.03; S, 2.28.

*[$Ag_2(\mu_3,\kappa^2$-SCN)(P^4)]$_2$(SCNB(C_6F_5)$_3$)$_2$ (**17**).* This compound was prepared similarly to **13** using complex **11** (38 mg, 0.017 mmol) and $B(C_6F_5)_3$ (18 mg, 0.035 mmol). It was recrystallized by gas phase diffusion of pentane into a tetrahydrofuran solution of **17** at +5 °C to give colorless crystals (40 mg, 86%). IR (KBr; ν(C≡N); cm^{-1}): 2158, 2124. $^{31}P\{^1H\}$ NMR (CD_2Cl_2; 298 K; δ): AB_3 spin system, −2.1 ($^3J_{PP}$ 175 Hz, $^1J_{AgP}$ 215 Hz, 3P), −34.5 ($^3J_{PP}$ 175 Hz, 1P). ^{19}F NMR (CD_2Cl_2; 298 K; δ): −166.1 (ddd, 6F, J_{FF} 23.2, 21.5, 7.8 Hz), −161.2 (t, 3F, J_{FF} 21.5 Hz), −134.9 (dd, 6F, J_{FF} 23.2, 7.8 Hz). ^1H NMR (CD_2Cl_2; 298 K; δ): 7.49 (m, 18H), 7.28−7.22 (m, 24H), 7.18−7.01 (m, 36H), 6.80 (m, 6H). Anal. Calcd for $C_{148}H_{84}Ag_4B_2F_{30}N_4P_8S_4{\cdot}2C_4H_8O$: C, 54.13; H, 2.91; N, 1.62; S, 3.71. Found: C, 54.52; H, 3.35; N, 1.69; S, 3.38.

DOI: 10.1021/acs.inorgchem.8b03166
Inorg. Chem. 2019, 58, 3646−3660

*[Ag(Xantphos)$_2$](SCNB(C_6F_5)$_3$) (**18**).* $B(C_6F_5)_3$ (32 mg, 0.0633 mmol) was added under nitrogen to a degassed solution of complex **4** (45 mg, 0.030 mmol) in freshly distilled THF (5 mL), and the mixture was refluxed for 4 h. The resulting clear, nearly colorless solution was evaporated, and the residue was washed with hexanes (2 × 5 mL). The solid was recrystallized by gas phase diffusion of pentane into its tetrahydrofuran solution to give a colorless crystalline material (40 mg, 73%). IR (KBr; ν(C≡N); cm^{-1}): 2152. $^{31}P\{^1H\}$ NMR (CD_2Cl_2; 298 K; δ): −8.28 (dd, $^1J_{107AgP}$ 238 Hz, $^1J_{109Ag-P}$ 265 Hz, 4P). ^1H NMR (CD_2Cl_2; 298 K; δ): 7.74 (dd, 4H, J_{HH} 8.1, 1.4 Hz, C_6H_3), 7.35 (t, 8H, J_{HH} 7.2 Hz, para-H Ph), 7.20 (dd, 4H, J_{HH} ca. 8.1 Hz, C_6H_3), 7.05−6.93 (m, 32H, meta- and para-H Ph), 1.57 (s, 12H, CH_3). Anal. Calcd for $C_{97}H_{64}AgBF_{15}NO_2P_4S$: C, 63.48; H, 3.52; N, 0.76; S, 1.75. Found: C, 63.12; H, 3.79; N, 0.87; S, 1.59.

X-ray Structure Determinations. The crystals of **1**−**12**, **13S**, and **15**−**17** were immersed in cryo-oil, mounted in a Nylon loop, and measured at a temperature of 150 K. The diffraction data was collected with Bruker SMART APEX II, Kappa Apex, and Bruker Kappa Apex II Duo diffractometers using Mo Kα radiation (λ = 0.71073 Å). The *APEX2*[27] program package was used for cell refinements and data reductions. The structures were solved by direct methods using the *SHELXS-2014*[28] program with the *WinGX*[29] graphical user interface. A semiempirical or numerical absorption correction (*SADABS*)[30] was applied to all data. Structural refinements were carried out using *SHELXL-2014/2018*.[28]

The SCN ligand in **8**, one $CF_3SO_3^-$ counterion in **12**, and a phenyl ring of the phosphine ligand in **16** were disordered between two positions each and were refined with occupation factors 0.51/0.49, 0.75/0.25, and 0.52/0.48, respectively. Geometry and displacement constraints and restraints were applied to these motifs. The crystallization solvent was lost from the crystals of **1**, **4**, **5**, **11**, **13S**, **15**, and **17** and could not be resolved unambiguously. The contribution of the missing solvent to the calculated structure factors was taken into account by using a SQUEEZE[31] routine of PLATON.[32] The missing solvent was not taken into account in the unit cell content. All hydrogen atoms in the studied structures were positioned geometrically and constrained to ride on their parent atoms, with C−H = 0.95−0.99 Å, U_{iso} = 1.2−1.5U_{eq} (parent atom). The crystallographic details are summarized in Table S1 in the Supporting Information.

Photophysical Measurements. Emission and excitation spectra in solution for complexes **10** and **13**−**16** were recorded on a FluoroMax 4 (JY Horiba Inc.) spectrofluorometer in a 1 cm quartz cuvette (freshly distilled tetrahydrofuran, concentration ca. 10^{-5} M, 298 K). The emission quantum yields in solution were determined under oxygen-free conditions by a comparative method using LED 365 nm as excitation source and Rhodamine 6G in ethanol (Φ = 95%) as the reference dye.[33] The steady-state emission and excitation spectra of complexes **1** and **5**−**17** in the solid state at 298 K and at 77 K were measured on HR2000 (Ocean Optics), FluoroLog 3, and FluoroMax 4 (JY Horiba Inc.) spectrofluorometers. The xenon lamps (300 and 450 W) served as excitation sources. The pulse laser DTL-399QT "Laser-export Co. Ltd" (351 nm, 50 mW, pulse width 6 ns, repetition rate 1 kHz), a monochromator MUM (LOMO, bandwidth of slit 1 nm), photon counting head H10682 (Hamamatsu), and multiple-event time digitizer P7887 (FAST ComTec GmbH) were used for lifetime measurements. The samples were placed in a cryostat optCRYO 105 for measurements in the temperature range 77−270 K. The absolute emission quantum yields of solid samples, which were loaded in Teflon cuvettes and covered by a quartz glass ring, were measured using a FluoroLog 3 (JY Horiba Inc.) spectrofluorometer and a Quanta-phi integration sphere (Horiba).

Computational Details. Quantum chemical calculations were carried out using the Gaussian 16 program package[34] at the (TD-)DFT level of theory. The PBE0[35,36] hybrid density functional was utilized throughout the study, combined with the def2-TZVPPD[37] basis set for the metal atoms; 6-311+G(d) basis set for P, N, S, and B atoms; and 6-31G(d) basis set for C, H, and F atoms. Frequency calculations were carried out for the optimized S_0, T_1, and S_1 geometries to confirm that the optimized structures correspond to a minimum on the potential energy surface. $\Delta E(S_1-T_1)$ values were estimated from the total energy differences optimized at the TD-DFT level. For **16**, $\Delta E(S_1-T_1)$ was estimated as the difference in the vertical $S_0 \rightarrow S_1$ and $S_0 \rightarrow T_1$ excitations, due to convergence issues during optimization.

RESULTS AND DISCUSSION

Synthesis and Characterization. *Diphosphine Dinuclear Complexes.* The reactions of commercially available chelating diphosphines $\mathbf{P^2}$, bis[(2-diphenylphosphino)phenyl] ether (DPEphos), 4,5-bis(diphenylphosphino)-9,9-dimethylxanthene (Xantphos), and 1,2-bis(diphenylphosphino)benzene (dppb), with copper thiocyanate in a 1:1 molar ratio, were carried out under an inert atmosphere in a refluxing methanol−dichloromethane mixture, following the previously reported protocols (Scheme 1, see the Experimental Section for the details).[38,39]

Scheme 1. Diphosphine Ligands and the Corresponding Dinuclear Complexes 1−6

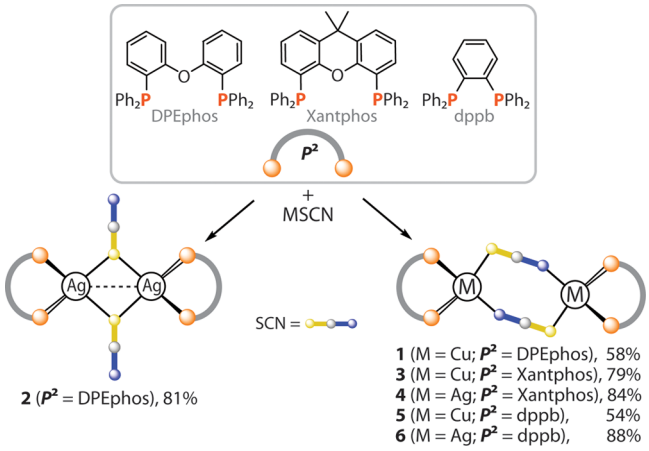

The target products of the general formula $[Cu(SCN)\mathbf{P^2}]_2$ ($\mathbf{P^2}$ = DPEphos, **1**; Xantphos, **3**; dppb, **5**) were obtained as pale crystalline materials in moderate yields (54−79%) due to the formation of virtually insoluble materials of undefined composition. The analogous silver compounds $[Ag(SCN)\mathbf{P^2}]_2$ ($\mathbf{P^2}$ = DPEphos, **2**; Xantphos, **4**; dppb, **6**) were prepared in a similar straightforward way although more efficiently (81−88%).

The single crystal diffraction analysis confirms that compounds **1**−**6** adopt the dimeric molecular structures (Figure 1 and Figure S1, with the crystallographic data and the selected structural parameters listed in Tables S1 and S2 in Supporting Information). In all these complexes except **2**, the thiocyanate ligands are coordinated in a μ_2,κ^2-mode and bridge two metal centers to give the $M\binom{SCN}{NCS}M$ metallacycles, which have been previously observed for the related copper(I) and silver(I) species.[38−44] A copper complex that is nearly identical to **5**, having a diphosphine ligand with *o*-tolyl substituents on one phosphorus center, has been structurally characterized earlier.[45] The diphosphine ligands complete the distorted tetrahedral geometry of each metal ion and are bound to the $M\binom{SCN}{NCS}M$ motifs in a *trans*-manner in centrosymmetric molecules of **1** and **4**−**6**. Due to this arrangement, which evidently minimizes the intramolecular steric hindrance, the

DOI: 10.1021/acs.inorgchem.8b03166
Inorg. Chem. 2019, 58, 3646−3660

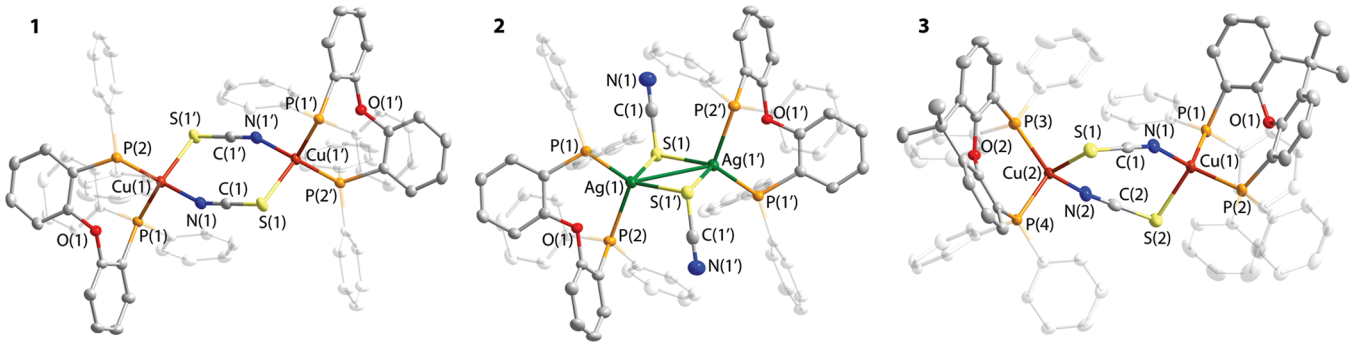

Figure 1. Molecular views of complexes **1**–**3** (one of two independent molecules found in the unit cell of **1** is presented). Thermal ellipsoids are shown at the 50% probability level. H atoms are omitted for clarity.

Scheme 2. Preparation of Complexes 7–12 Based on Tri- and Tetraphosphine Ligands P^3 and P^4

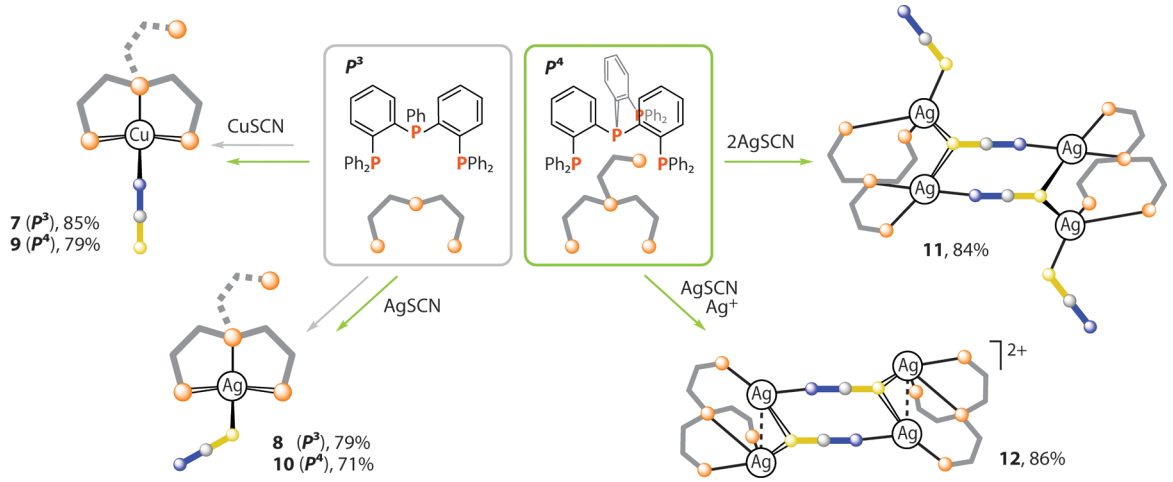

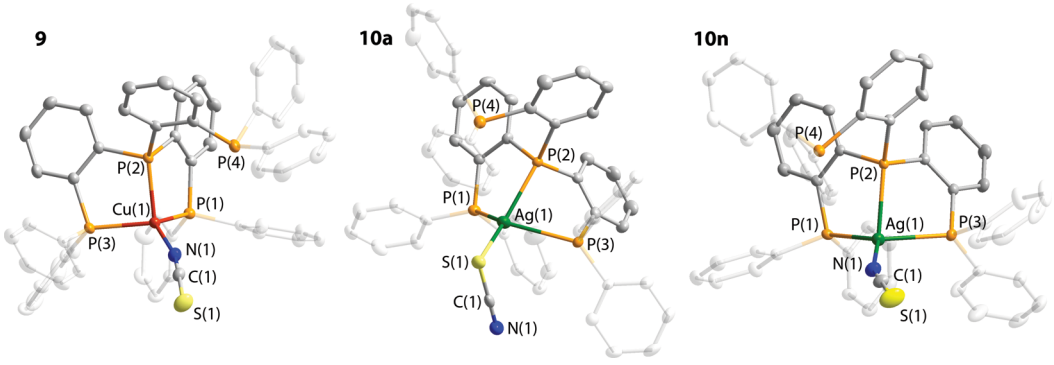

Figure 2. Molecular views of complexes **9** (ether solvate), **10a**, and **10n**. Thermal ellipsoids are shown at the 50% probability level. H atoms are omitted for clarity.

thiocyanate metallorings appear as nearly planar (**6**) or chairlike conformations (**1**, **4**, and **5**). In **3**, however, the Xantphos ligands are found in a *cis*-position that decreases the molecular symmetry and leads to the twisting distortion of the $Cu\binom{SCN}{NCS}Cu$ fragment apparently because of some repulsion between the phosphine phenyl rings.

In the disilver complex **2**, thiocyanate groups are bound to the metal centers in a more rare μ_2,κ^1-manner via the sulfur atoms leading to a short Ag–Ag distance of 3.2116(3) Å that is considerably below the sum of two van der Waals radii for silver (3.44 Å). Nevertheless, the same coordination mode observed for $[Ag(SCN)(dppf)]_2$ and $[Ag(SCN)(dpam)]_n$ (dppf = bis(diphenylphosphino)ferrocene; dpam = diphenylarsinomethane) compounds[40,46] resulted in substantially longer metal–metal separations (3.703 and 3.820 Å, respectively) suggesting a non-negligible role of the packing effect on the structural features. In general, the values of bond lengths and angles determined for **1**–**6** (Table S2) are typical for this sort of complex and correlate well with the reported data.[38–44,46]

The solid-state IR spectra of **1**–**6** reveal a strong peak from the SC≡N stretching vibration in between 2088 and 2108 cm^{-1} that is comparable to those of other Cu(I) and Ag(I) thiocyanate-bridged compounds.[39,42–44,46] The ^1H NMR spectra of these dinuclear complexes recorded at ambient

DOI: 10.1021/acs.inorgchem.8b03166
Inorg. Chem. 2019, 58, 3646–3660

temperature mostly display broad and unresolved signals thus providing rather limited structural information. The presence of one ^{31}P NMR signal for each compound points to the equivalence of all phosphorus atoms in the molecules in solution due to stereochemical nonrigidity at room temperature. The doublet resonances are observed in the phosphorus spectra of the silver species **2** and **4** (J_{P-Ag} = 366 and 374 Hz, respectively; the splittings due to ^{107}Ag and ^{109}Ag isotopes are not distinguishable at 298 K); the coupling constants are within the range found earlier for the structurally similar complexes.[42,46]

Tri- and Tetraphosphine Mononuclear Complexes. Treatment of copper and silver thiocyanates with higher denticity phosphines **P^3** and **P^4** (Scheme 2) expectedly afforded monometallic products [CuNCS(**P^3**/**P^4**)] (**7**, **9**) and [AgSCN(**P^3**/**P^4**)] (**8**, **10**) under mild conditions (Scheme 2). In the case of **10** an excess of tetraphosphine **P^4** (ca. 25 molar %) was used to prevent the formation of the tetranuclear complex **11** (see below).

The metal ions in **7**−**10** are found in a typical pseudotetrahedral environment, formed by three P-donor functions, provided by the **P^3**/**P^4** phosphines, and the SCN ligand (Figure 2 and Figure S2, and Tables S3 and S4 summarize structural details). The latter is coordinated via the N atom in copper complexes **7** and **9**, which was isolated as yellow-greenish diethyl ether solvate **9**, yellow unspecified solvate **9a**, and a minor yellow-orange solvent-free form **9b**, see the Supporting Information. In the silver relative **8** and in most of the obtained forms of **10**, the thiocyanate anion is connected to the metal center through the sulfur atom (Figure 2 and Figure S2).

Complex **10** revealed an unusual diversity of crystalline forms, which also show distinctly different optical features (*vide infra*). Thus, in addition to the solvent-free modifications **10** (pale greenish) and **10a** (yellow), this compound was characterized as tetrahydrofuran (**10b**) and methanol solvates (**10c**). The greenish nonsolvated pseudopolymorph **10**, which could be obtained in small quantities and with poor reproducibility, is supposedly a metastable form of **10a**; both crystallize in the same type of spacegroup ($P2_1/c$) with very similar unit cell parameters (Table S1). Moreover, crystallization of **10** from THF/acetonitrile or pure acetonitrile selectively produces linkage isomer **10n**, where the SCN group is N-bound to the silver atom (Figure 2).

The difference in coordination of the SCN ligand in mononuclear complexes **7**−**10** is clearly reflected by the magnitude of ∠M−E−C, which tends to approach a right angle for E = S (89°−110° for **8** and forms of **10**) compared to the values of 166.0−175.5° for E = N in **7** and the family of **9**. This variation in bonding of the SCN anion generally complies with the literature data on d^{10} [M(SCN)(PR$_3$)$_3$] compounds.[39,42,47]

In all forms of complexes **9** and **10**, the tetraphosphine **P^4** phosphine serves as a tridentate ligand leaving one terminal PPh_2 function unbound (Cu(1)−P(4) and Ag(1)−P(4) separations are 4.101 Å and 3.848/3.979 Å, Figure 2), analogously to their alkynyl congener [Cu(C$_2$Ph)(**P^4**)].[26] The geometry of {M(P)$_3$} skeletons and the structural characteristics in **7**−**10** (Tables S3 and S4) closely resemble those of other [M(**P^3**)X] compounds.[25,48,49]

The C≡N stretching frequencies of compounds **8** and **10**(**a**, **b**) with a bent geometry of the Ag−SCN fragments (2097 and 2092 cm^{-1}) are systematically higher than those for **7** and **9** with N-coordinated thiocyanates (2080 and 2083 cm^{-1}) that agree with earlier observations[39,42] and confirm the presence of one coordination isomer in the bulk sample.

The ^{31}P NMR spectra of triphosphine complexes **7** and **8** at room temperature display two broad and poorly resolved signals with 2:1 ratio of integral intensities, which correspond to two types of phosphorus atoms in symmetrically coordinated **P^3** ligand. In the case of **8**, only the low field resonance of the PPh_2 groups reveals P−Ag coupling (J_{P-Ag} = ca. 206 Hz) that, together with the broadness of spectroscopic profiles, indicates a substantial nonrigidity of these compounds in solution. Copper complex **9** also undergoes dynamic processes under ambient conditions as its ^{31}P spectrum shows one unresolved multiplet. The spectrum at 193 K displays four signals of equal intensity (Figure S3). Three of them are broadened because of direct coordination of the phosphorus functions to quadrupolar copper nuclei, whereas the fourth resonance corresponds to the dangling PPh_2 group and appears as a resolved multiplet due to coupling with the other phosphorus nuclei that evidently corresponds to the structure found in the solid state. The silver analogue, however, demonstrates the AX_3 spectroscopic pattern in the ^{31}P spectrum (Figure S3), additionally split due to P−^{107,109}Ag couplings ($^1J_{P\text{-}107Ag}$ = 179 and 112 Hz, $^1J_{P\text{-}109Ag}$ = 203 and 129 Hz), suggesting that in solution the **P^4** phosphine is symmetrically bound to the metal ion as a result of possible dissociation of SCN anion. This hypothesis is also supported by the crystallization of two isomers **10**(**a**, **b**) and **10n**, the formation of which requires cleavage of Ag−S or Ag−N bonds in solution.

Tetraphosphine Tetranuclear Complexes. Increasing the amount of starting AgSCN in the reaction with **P^4** leads to the assembly of the neutral tetranuclear cluster [Ag$_2$(μ_3,κ^2-SCN)(t-SCN)(**P^4**)]$_2$ (**11**), whereas using the 1:1 mixture of AgSCN/AgCF$_3$SO$_3$ generated the dicationic cognate [Ag$_2$(μ_3,κ^2-SCN)(**P^4**)]$_2$(CF$_3$SO$_3$)$_2$ (**12**), see Scheme 2. The structural motif of these aggregates, depicted in Figure 3, is reminiscent of that of the cyanide complexes [M$_2$(CN)(**P^4**)]$_2^{2+}$.[50] Both **11** and **12** contain 8-membered thiocyanate metalloring decorated with additional silver ions, which are appended to the sulfur atoms to give a chairlike configuration. The Ag−S bonds (2.532−2.556 Å, Table S5) within a flat $Ag\binom{SCN}{NCS}Ag$ core are systematically shorter than in dinuclear complexes **4** and **6** (2.608−2.682 Å) having the same framework, while the Ag−N contacts in **11** and **12** do not deviate substantially from those in diphosphine compounds. Cluster **11** does not show appreciable Ag···Ag contacts (the corresponding separation is 3.445 Å) due to the saturation of coordination vacancies of both metals. In **12**, which is derived from **11** by removing terminal SCN groups, the lack of the ligands causes a significant contraction of the silver−silver distance to 2.918−2.970 Å.

In solution compounds **11** and **12** exhibit fluxional behavior according to the ^{31}P NMR spectroscopic data (Figure S4), which reveal two resonances of 3:1 relative integral intensities arising from the fast motion of the tetraphosphine ligands and/or reversible dissociation/association, akin to the described behavior of [Ag$_2$(CN)(**P^4**)]$_2^{2+}$.[50]

Isothiocyanatoborate Complexes. Inspired by the reports on the modification of luminescent cyanide metal complexes by coupling with strong Lewis acid B(C$_6$F$_5$)$_3$ to generate isocyanoborate ligands,[51−53] we employed the mononuclear

DOI: 10.1021/acs.inorgchem.8b03166
Inorg. Chem. 2019, 58, 3646−3660

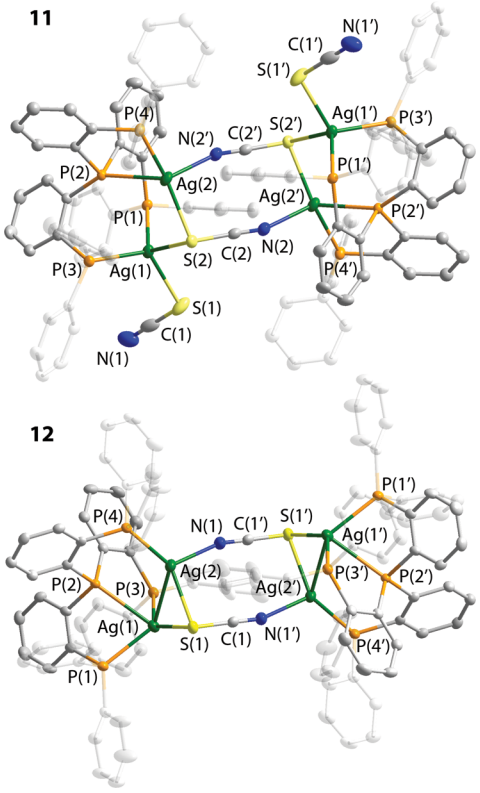

Figure 3. Molecular views of complexes **11** and **12** (one of two independent molecules found in the unit cell of **12** is presented). Thermal ellipsoids are shown at the 50% probability level. H atoms are omitted for clarity.

compounds **7**−**10** bearing terminally coordinated ambidentate thiocyanates in the analogous reactions. Thus, the interaction of **7**−**10** with $B(C_6F_5)_3$ in dry deaerated tetrahydrofuran results in a clean conversion of the parent complexes into the isothiocyanatoborate derivatives $[M\{SCN{:}B(C_6F_5)_3\}(\mathbf{P^3}/\mathbf{P^4})]$ (**13**−**16**) by attaching the borane fragment to the nitrogen atom of the SCN anion (Scheme 3).

Scheme 3. Preparation of Isothiocyanatoborate Complexes 13−**16**

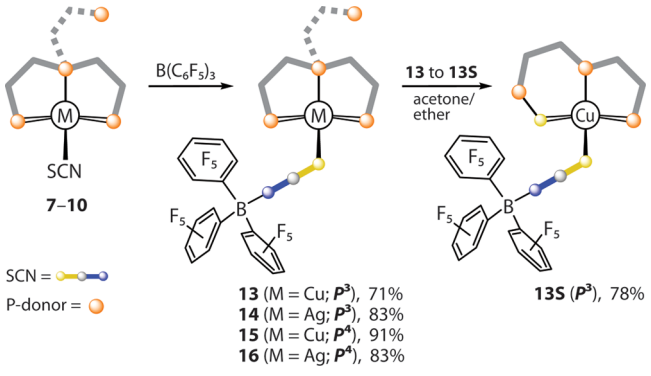

The $^{-}SCN{:}B(C_6F_5)_3$ adduct is formed selectively in the isothiocyanate form (see the structural discussion below), regardless of the initial bonding mode of SCN in the starting compounds that is in line with the concept of hard and soft acids and bases.[54] It is worth mentioning that, despite the isothiocyanatoborate anion having been described 15 years ago,[55,56] it was not previously utilized in the coordination chemistry of transition metal complexes.

Products **13**−**16** were isolated as readily soluble pale crystalline materials, which are generally stable toward moisture and oxygen. The only exception is the copper complex $[Cu\{SCN{:}B(C_6F_5)_3\}(\mathbf{P^3})]$ (**13**), which degrades upon crystallization in acetone/diethyl ether solution on air producing the $[Cu\{SCN{:}B(C_6F_5)_3\}(\mathbf{P^3S})]$ (**13S**) compound with partially sulfidated triphosphine; the latter is a unique example of a heterodentate P,P,S-ligand, which is formed evidently in the course of decomposition of the SCN group. The XRD data for compounds **13S**, **15**, and **16** confirm that the isothiocyanatoborate ligand is S-coordinated and the metal centers retain the typical tetracoordinate ligand sphere (Figure 4 and Figure S5, with the structural parameters summarized in

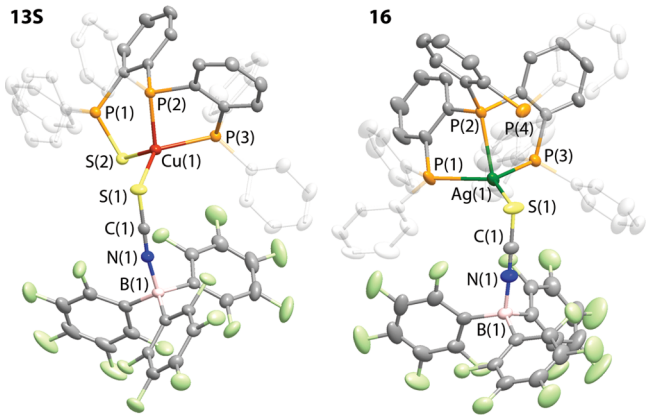

Figure 4. Molecular views of complexes **13S** and **16**. Thermal ellipsoids are shown at the 50% probability level. H atoms are omitted for clarity.

Table S6). In **13S** the S−Cu bonds involving the $Ph_2P{=}S$ group (2.304 Å) and the $SCN{:}B(C_6F_5)_3$ ligand (2.346 Å) are commensurate with the corresponding distances found in other copper thiocyanate[39,41,44] and phosphine−sulfide[57−59] compounds.

The stereochemistry of $SCN{:}B(C_6F_5)_3$ fragments in crystallographically identified compounds **13S**, **15**, and **16** is virtually identical to that described for the potassium salts $[K(18\text{-crown-}6)][SCN{:}BR_3]$[55,56] and reveals a nearly linear arrangement of SCNB atoms. The bonding of the borane group to the SCN anion causes some systematic shortening of the C≡N bond length (1.136−1.152 Å) with respect to those of the parent complexes **7**−**10** (d_{CN} = 1.152−1.160 Å) that also matches an increase in ν(CN) stretching frequencies in **13**−**16** (2189−2181 cm^{-1}) relative to **7**−**10** (2097−2080 cm^{-1}).

The copper-containing compound **15** was obtained in two crystalline modifications, a greenish tetrahydrofuran solvate **15** (spacegroup $C2/c$) and a yellow solvent-free material **15a** (spacegroup $P\bar{1}$), which is isomorphous to the silver analogue **16**.

It should be mentioned that the attempts to prepare the borane derivatives of other complexes were unsuccessful. The exposure of cluster **11**, bearing pendant thiocyanate ligands, to $B(C_6F_5)_3$ yields the salt $[Ag_2(SCN)(\mathbf{P^4})]_2(SCNB(C_6F_5)_3)_2$ (**17**) with noncoordinated $[SCN{:}B(C_6F_5)_3]^{-}$ counterion (Figure S5), the tetrametallic dication of which is essentially the same as in **12**. Furthermore, the dinuclear species **1** and **2**

DOI: 10.1021/acs.inorgchem.8b03166
Inorg. Chem. 2019, 58, 3646−3660

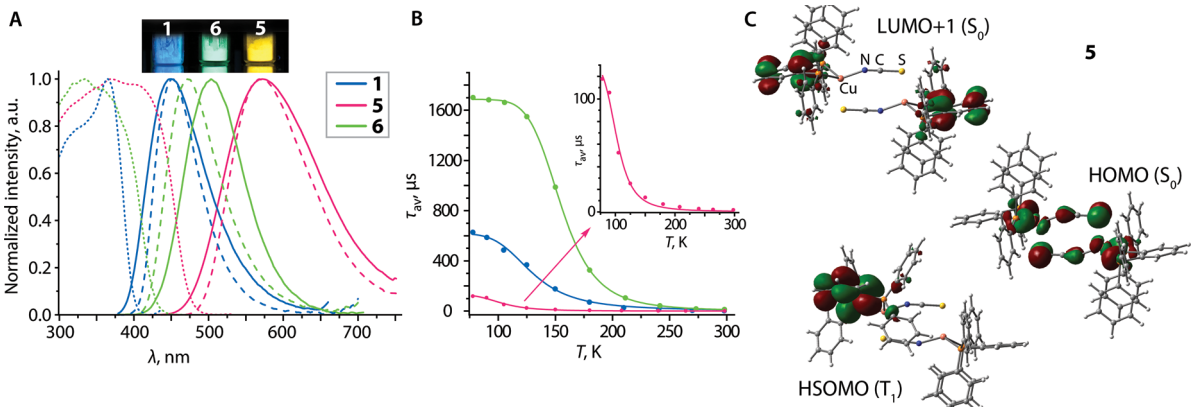

Figure 5. (A) Normalized solid-state excitation (dotted lines, 298 K) and emission spectra (solid lines, 298 K; dashed lines, 77 K) of **1**, **5**, and **6** (the photograph shows their appearance under UV light at 298 K). (B) Temperature dependencies of average lifetimes of **1**, **5**, and **6** (the solid lines are the fits according to eq 1). (C) Frontier orbitals in the ground state (S_0) and the highest singly occupied molecular orbital of the lowest excited triplet state (T_1) of complex **5** (optimized geometries, the distribution of LUMO is almost identical to that of L + 1).

Table 1. Solid-State Photophysical Properties of Complexes 1 and 5−17[a]

	298 K						77 K		
	λ_{em}, nm	Φ, %	τ_{obs}, μs	τ_{av}, μs	k_r, s^{-1}	k_{nr}, s^{-1}	λ_{em}, nm	τ_{obs}, μs	τ_{av}, μs
1	448	15	3.2 (35.3), 0.7 (64.7)	2.5	5.9×10^4	3.4×10^5	452	125.5 (39.6), 707.9 (61.4)	628.8
5	571	14	1.8		7.5×10^4	4.8×10^5	571	117.7	
6	505	35	4.3 (26.5), 12.9 (73.5)	12.0	2.9×10^4	0.5×10^5	472	623.8 (53.7), 2074.8 (46.3)	1700.6
7	520	57	0.9 (50.0), 5.4 (50.0)	4.8	1.2×10^5	0.9×10^5	520	114.1 (33.0), 738.4 (67.0)	694.3
8	538	32	5.5 (27.7), 16.2 (72.3)	15.0	2.1×10^4	0.5×10^5	548	1224.4 (70.0), 691.7 (30.0)	1120.6
9	543	27	1.3 (37.8), 5.4 (62.2)	4.9	5.5×10^4	1.5×10^5	552	610.8 (9.9), 1423.8 (90.1)	1386.8
9a	575	23	0.9 (16.3), 3.9 (83.7)	3.8	6.0×10^4	2.1×10^5	575	332.8 (29.8), 1133.5 (70.2)	1044.7
10a	552	27	2.2 (20.0), 10.5 (80.0)	10.1	2.7×10^4	0.7×10^5	507	450.8 (78.4), 1163.1 (21.6)	746.9
10c	630	19	3.5 (17), 7.2 (84)	6.9	2.8×10^4	1.2×10^5	645	346.3 (44), 1032.3 (56)	890.2
10n	525	44	5.4 (27.9), 11.0 (72.1)	10.1	4.3×10^4	0.6×10^5	518	389.7 (17.0), 625.0 (83.0)	598.4
11	468	43	6.9 (71.4), 2.0 (28.6)	6.4	6.7×10^4	0.9×10^5	478	259.8 (26.0), 803.4 (74.0)	747.9
12	475	11	1.3 (61.0), 4.7 (39.0)	3.7	3.0×10^4	2.4×10^5	498	50.7 (54.9), 259.7 (45.1)	219.6
13	505	39	7.9 (13.9), 18.3 (86.1)	17.6	2.1×10^4	3.4×10^4	515	3245.1 (77.6), 939.2 (22.4)	3067.2
14	482	12	24.1 (85.7), 10.1 (14.3)	23.2	0.5×10^4	3.8×10^4	478	1658.2 (62.6), 506.7 (37.4)	1480.4
15	505	17	2.5 (54.3), 0.4 (45.7)	2.3	7.4×10^4	3.7×10^5	500	203.8 (37.7), 2089.1 (62.3)	1983.9
15a	625	11	1.6 (48.2), 4.7 (51.8)	4.0	2.7×10^4	2.3×10^5	666	1336.7 (75.2), 238.5 (24.8)	1275.8
16	575	9	9.3 (52.9), 2.3 (47.1)	8.0	1.1×10^4	1.1×10^5	630	1127.3 (63.9), 306.1 (36.1)	1018.1
17	470	4	7.1 (63.9), 2.2 (36.1)	6.4	6.3×10^3	1.5×10^5	460		

[a]The uncertainty of the quantum yield measurement is in the range of ±5% (an average of three replica). Average emission lifetime for the two-exponential decay $\tau_{av} = (A_1\tau_1^2 + A_2\tau_2^2)/(A_1\tau_1 + A_2\tau_2)$. A_i = weight of the i exponent. $k_r = \Phi/\tau_{av}$. $k_{nr} = (1 - \Phi)/\tau_{av}$.

appeared to be inert toward $B(C_6F_5)_3$, while in the case of **4** the reaction leads to the cleavage of its dimeric structure and the formation of the bis-diphosphine complex $[Ag(Xantphos)_2](SCNB(C_6F_5)_3)$ (**18**, Figure S5), recently described with the BF_4^- anion.[60]

The NMR spectroscopic data for compounds **13−16** are compatible with those for the parent complexes **7−10** and with the crystal structures of **15** and **16** (see Experimental Section). The ^{31}P spectrum of **13** at 298 K shows two broadened resonances in a 2:1 ratio and the chemical shifts akin to those of **7**. Complex **15** at room temperature demonstrates one ^{31}P signal and proved to be more fluxional than **9**; the dynamic processes were not frozen even at 193 K. Although silver compounds **14** and **16** already at room temperature demonstrate well-resolved ^{31}P patterns, these were interpreted as AB_2 and AX_3 spin systems with characteristic $P-^{107,109}Ag$ splittings (Figure S6). The ^{31}P spectroscopic profile of **16** is identical to that of **8** (see Figures S4 and S6) that also suggests a symmetric coordination of the tetraphosphine and a weak coordination of the $[SCN:B(C_6F_5)_3]^-$ ligand in solution. The phosphorus NMR spectrum of complex **13S** reveals three multiplets (1:1:1 intensities ratio) as anticipated from the P,P,S-coordinated diphosphine-phosphine sulfide ligand (Figure S7). All compounds with the $B(C_6F_5)_3$ fragment display very similar ^{19}F NMR spectra, assigned to the *ortho-*, *meta-*, and *para*-fluorine atoms of the equivalent C_6F_5 rings.

Photophysical Properties and Computational Studies. Among the titled complexes, **2−4** and **13s** do not show appreciable luminescence. Furthermore, the optical studies of the other compounds were mainly performed in the solid state due to the aforementioned dynamics and generally very weak photoemission in solution.

The dinuclear copper complexes **1** and **5** show blue and yellow moderately intense emission, the energy of which remains virtually the same at 77 K (Figure 5 and Table 1). Their lifetimes are dramatically increased upon cooling and feature nonlinear temperature dependencies typical for TADF behavior. Fit of these data by using eq 1, that takes into

DOI: 10.1021/acs.inorgchem.8b03166
Inorg. Chem. 2019, 58, 3646−3660

account thermally equilibrated lowest triplet and singlet excited states, provides their intrinsic phosphorescence and fluorescence lifetimes $\tau(T_1)$ and $\tau(S_1)$ and the value of energy gap $\Delta E(S_1-T_1)$, which are listed in Table 2 along with

Table 2. Excited State Characteristics from the Fit Based on the Two-State Model and Theoretically Predicted Energy Gaps ($\Delta E(S_1-T_1)_{calc}$)

	$\Delta E(S_1-T_1)$, cm^{-1}	$\Delta E(S_1-T_1)_{calc}$, cm^{-1}	$\tau(T_1)$, μs	$\tau(S_1)$, ns
1	644	1129	618	184
5	572	1613	131	15
6	1111	726	1686	21
7	649	807	700	89
8	838	485	1117	119
9	*a*	1694		
10a	858	968	738	48
10c	740		883	79
10n	922	1774	597	28
11	910	565	749	41
13	697	1129	3083	20
14	1608	1291	1466	0.2
15	*a*	1291		
15a	691		1282	92
16	727	1694[b]	1005	19

[a]Could not be calculated by eq 1 due to growing τ_{obs} at 77 K. [b]Estimated as the energy difference between vertical $S_0 \rightarrow S_1$ and $S_0 \rightarrow T_1$ excitations.

computationally assessed energy separations $\Delta E(S_1-T_1)_{calc}$. The latter parameters, although compatible with energetics that favors delayed fluorescence, visibly deviate from the experiment-based data, at least in part, eventually because of the crystal lattice effects.

$$\tau(T) = \frac{3 + \exp\left[-\frac{\Delta E(S_1-T_1)}{k_B T}\right]}{\frac{3}{\tau(T_1)} + \left[\frac{1}{\tau(S_1)}\right]\exp\left[-\frac{\Delta E(S_1-T_1)}{k_B T}\right]} \quad (1)$$

Due to a relatively small separation between the S_1 and T_1 levels (644 and 572 cm^{-1} for **1** and **5**), the higher lying S_1 state is still in part thermally populated even at 77 K as indicated by the lifetime, which does not reach the plateau region at this temperature.

With the consideration of the structural similarity of **1** and **5**, the drastic difference in their emission colors might be determined by the nature of the diphosphine ligands (DPEphos and dppb). Computational analysis of the electronic structures of these compounds shows that the lowest energy excitations $S_0 \rightarrow S_1$ are virtually forbidden (oscillator strength $f = 0$) but are very close energetically to the allowed $S_0 \rightarrow S_n$ ($n > 1$) electronic transitions (Table S7), which predominantly involve HOMO and LUMO + 1 (S_2, **1**) or LUMO + 1/+ 3 (S_3 and S_4, **5**). The HOMO contains the contributions of the copper and phosphorus atoms mixed with NCS ligands, while the higher lying unoccupied orbitals are located on the aromatic spacers of the diphosphines (Figure 5c and Figure S8, and Table S8). Furthermore, the highest singly occupied orbital of the triplet state is also displaced on the P-ligand backbone, and therefore, both S_1 and T_1 states have a mixed (Cu + NCS) $\rightarrow \pi$(phosphine) charge transfer character, i.e., (M + L′)LCT. This active role of rather structurally flexible bimetallic metallocycles might account for moderate quantum yields of these compounds, which show visibly larger nonradiative rate constants than most of the other species (Table 1). Notably, the luminescence properties of **5** considerably diverge from the behavior of its close congener $[Cu(SCN)(PPh_2C_6H_4PTol_2)]_2$,[45] which was reported to show blue emission (λ_{em} = 478 nm vs 571 nm for **5** at 298 K) and substantially longer lifetimes (τ_{obs} = 4.7 μs at 298 K, 1077 μs at 77 K vs 1.8 μs at 298 K, 118 μs at 77 K for **5**). In a view of nearly identical electronic features of the ligands in these compounds, such a deviation of the photophysical characteristics points to their significant dependence on an intramolecular steric effect and the solid-state packing.

The silver analogue of **5**, complex **6**, also demonstrates delayed fluorescence under ambient conditions with a somewhat larger $\Delta E(S_1-T_1)$ value of 1111 cm^{-1} and hypsochromically shifted emission (λ_{em} = 505 nm) in comparison to that of **5** (λ_{em} = 571 nm). The latter effect correlates with higher oxidation potential for Ag^I vs Cu^I. According to DFT calculations, the change of Cu for Ag results in 0.2 eV stabilization of HOMO in **6** (0.16 eV increase of the HOMO−LUMO gap). Simultaneously, the composition of the frontier molecular orbitals shows that the metal centers and NCS ligands in **6** constitute 20% and 34% of the HOMO, respectively (30% and 28% in **5**, Table S8), indicating a larger proportion of L′LCT vs MLCT for the silver complex (see also the frontier orbital plots in Figure S9). In contrast to a majority of TADF luminophores, the emission energy of **6** is noticeably increased at 77 K (λ_{em} = 472 nm vs 505 nm at 298 K), and a similar effect is observed for **10a**, **10n**, **14**, and **15** (see below). A similar behavior was reported for some other crystalline complexes with the TADF property[16,61,62] and has been tentatively attributed to possible stabilization of the ground state at low temperature via intermolecular interactions, and to the rise of the excited state energy due to restrained structural distortions in the frozen crystal. The latter hypothesis is supported by the analysis of theoretically optimized relaxed geometries for **6** in the ground (S_0) and excited states (S_1 and T_1). As can be seen in Figure S10, both $S_0 \rightarrow S_1$ and $S_0 \rightarrow T_1$ excitations break the symmetry of the molecule and lead to a substantial flattening of coordination geometry of one silver atom that is accompanied by some contraction of the metal−ligand bond distances. Consequently, the excited molecule is predicted to undergo a severe twist (the angle between the planes of phenylene spacer changes from 0° in S_0 to ca. 74° in S_1 and 72° in T_1) that is expected to be largely suppressed at 77 K and thus increases the energy gap.

The behavior of mononuclear triphosphine compounds [MSCN($\mathbf{P^3}$)] **7** (M = Cu) and **8** (M = Ag) at ambient temperature agrees with the data for their cyanide and halide relatives.[25,49] The predicted $S_0 \rightarrow S_1$ excitation corresponds mainly to the HOMO → LUMO transition (Table S7), which has the L′LCT (SCN → $\pi\mathbf{P^3}$) origin mixed with some metal to ligand ($\mathbf{P^3}$) charge transfer. As shown in Figure S11 and Table S8, the HOMO is primarily located on the thiocyanate ligand (76% for **7** and 66% for **8**), whereas the contribution of metal d orbitals amounts only to 10% (**7**) and 9% (**8**). Both complexes exhibit greenish delayed fluorescence (λ_{em} = 520 nm, **7**; 538 nm, **8**) with quantum yields for the neat crystalline sample reaching 33% (**8**) and 57% (**7**); the latter value is the highest one among the title complexes described in the present work. Also, the radiative rate constant for **7** ($k_r = 1.2 \times 10^5$ s^{-1}) is the largest within this series, resulting in an appreciably shorter TADF lifetime (4.8 μs) in comparison to those of

DOI: 10.1021/acs.inorgchem.8b03166
Inorg. Chem. 2019, 58, 3646−3660

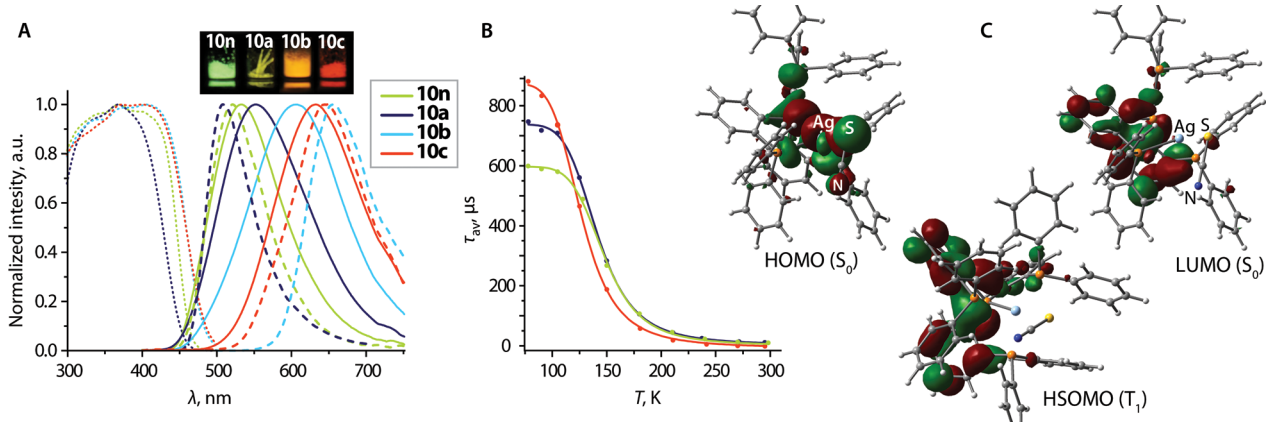

Figure 6. (A) Normalized solid-state excitation (dotted lines, 298 K) and emission (solid lines, 298 K; dashed lines, 77 K) spectra of **10**(**a**–**c**) and **10n** (the photograph shows their appearance under UV light at 298 K). (B) Temperature dependencies of average lifetimes of **10a**, **10c**, and **10n** (the solid lines are the fits according to eq 1). (C) Frontier orbitals in the ground state (S_0) and the highest singly occupied molecular orbital of the lowest excited triplet state (T_1) of **10** (optimized geometries).

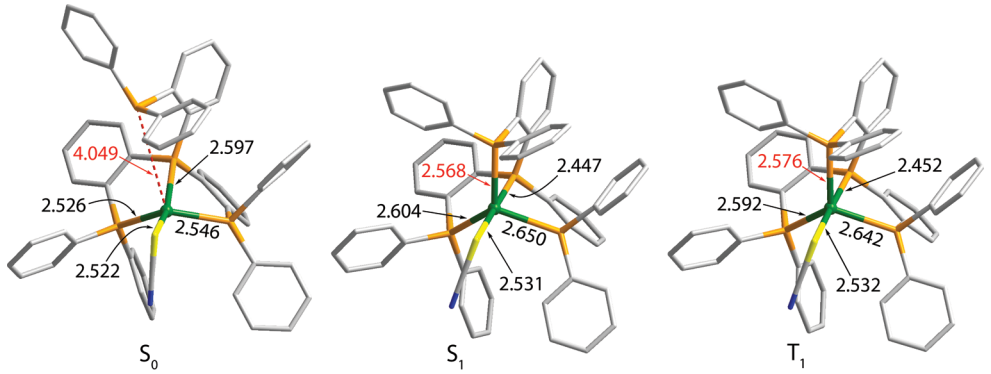

Figure 7. Relaxed geometries of S_0, S_1, and T_1 states for complex **10** (the indicated interatomic distances are given in Å).

congener species [Cu(**P**^{3})X] (X = Hal, τ_{obs} = 9.0–11.7 μs; CN, τ_{obs} = 15.4 μs).[25,49]

For complex [CuNCS(**P**^{4})] (**9**), which has been structurally characterized in three crystalline forms, we were able to investigate the optical properties for solvates **9** and **9a**. In the case of silver analogue **10**, the extensive sets of measurements were performed for the yellow solvent-free form **10a**, methanol solvate **10c** and the linkage isomer **10n**. For the sample **10b**, which exists as a mixture of at least two pseudopolymorphs, only the emission spectra were recorded. The nonsolvated modifications **9b** and **10**, which could not be isolated reproducibly and in sufficient quantities, were therefore excluded from further investigations. Likewise, as for the triphosphine relatives, the lowest energy transition $S_0 \rightarrow S_1$ (f = 0.017–0.024) for compounds **9**, **10**, and **10n** occurs mostly between the HOMO and LUMO (90%, 96%, and 81%, Table S7). Compared to those of **7** and **8**, the metal ions in **9** and **10** contribute 14% and 20% to the HOMO, respectively, meaning that the lowest excited states S_1 and T_1 for the tetraphosphine compounds have a more pronounced MLCT character (Figure 6 and Figure S12) along with ligand to ligand (SCN $\rightarrow$ π**P**^{3}) charge transfer. In addition, in **10**, where the SCN ligand is S-bound to the silver ion, the thiocyanate contribution to the HOMO decreases to 26% (64% for **9**) which is compensated by the HOMO distribution over the P atoms (54%, Table S8). Conversely, in **10n** the $S_0 \rightarrow S_1$ excitation refers to the dominating L′LCT process that is manifested by the corresponding localizations of HOMO (SCN, 81%; d_{Ag}, 5%) and LUMO (**P**^{3} ligand, 95%), see Figure S13 and Table S8.

Both forms **9** and **9a** emit in a yellow region with moderate intensity (Table 1 and Figure S12). Temperature dependence of the observed lifetime for **9** (Figure S11) in the 77–298 K window could not be adequately treated with eq 1 due to continuing growth of τ_{obs} at 77 K. Nevertheless, it is compatible with TADF behavior and points toward the S_1 and T_1 states being very close in energy (conceivably, less than 500 cm^{-1}). Theoretical studies though predict a rather large $\Delta E(S_1-T_1)$ separation of 1694 cm^{-1} for complex **9** that considerably exceeds the values for other mononuclear compounds (Table 2). The plausible reason for this discrepancy may arise from drastic geometry changes, which accompany the formation of the triplet state, computationally assessed in the gas phase (Figure S14). In particular, the P···Cu distance involving the noncoordinated PPh_2 group decreases from 3.980 Å in S_0 (the experimental value is 4.101 Å for **9**) to 3.447 Å in the S_1 state and further drastically contracts to 2.472 Å as a result of the transition to the T_1 state. Apparently, such structural variation might be considerably confined in the crystal, causing a certain destabilization of the T_1 level and therefore a narrowing of the $\Delta E(S_1-T_1)$ gap. For **10n**, the overall trend of geometry distortions follows that of **9** (Figure S14).

The family of crystalline materials formed by complex **10** reveals versatile luminescence properties (Figure 6). The nonsolvated isomer **10n** exhibits green emission (λ_{em} = 525

DOI: 10.1021/acs.inorgchem.8b03166
Inorg. Chem. 2019, 58, 3646–3660

nm), while yellow form **10a** emits at lower energy (λ_{em} = 552 nm). The solvated modifications **10b** (THF solvates) and **10c** (MeOH solvate) demonstrate additional bathochromic shifts of the emission maxima (λ_{em} = 605 and 630 nm, respectively) and thus reach a red-orange color for **10c**. The delayed fluorescence was confirmed for the samples **10a**, **10c**, and **10n**; like complex **6**, both solvent-free species **10a** and **10n** show a noticeable blue shift of the emission maxima when cooled to 77 K (Figure 6). Nevertheless, the onsets of the emission bands appear at longer wavelengths at lower temperatures, in line with the TADF mechanism.[16,61,62]

The significant variation of emission energies, which cover a wide range of the visible spectrum, can be tentatively interpreted in terms of structure distortions occurring in the excited states. Like congeners **9** and **10n**, complex **10** experiences dramatic photoinduced reorganization, which is geometrically quite similar for both S_1 and T_1 states and features a 5-coordinate trigonal bipyramidal environment of the metal center as indicated by the TD-DFT calculations (Figure 7). The lattice restraints therefore are expected to influence the luminescence color via altering the energy of the S_1 state, from which the radiative relaxation at room temperature occurs in the case of TADF.

The substantially red-shifted emission of complex **10**, observed in a nonrigid fluid medium (degassed tetrahydrofuran solution, λ_{em} = 690 nm at 298 K, Φ_{em} = 2.1%, Figure S15), correlates with this hypothesis. It also has been noted for other Cu and Ag compounds that their photophysical behavior can be altered by quite subtle structural changes,[21] and even two independent molecules in the unit cell are capable of showing different emissions.[63] The low quantum yield of **10** in solution is not surprising as large structural distortions occurring in the excited state typically facilitate its nonradiative deactivation.[21,64] In addition, mechanical grinding converts all modifications of **10** into essentially the same type of amorphous solid with yellow-orange luminescence. Exposure to acetonitrile transforms this phase into a pale microcrystalline material with intense greenish emission that implies the formation of the isomer **10n** (Figure 8).

The tetranuclear species **11** and **12** are blue luminophores (λ_{em} = 468 and 475 nm, Figure 9) with quantum yields of 43% and 11%. The neutral complex **11**, which demonstrates longer metal−metal separations than **12** in the ground and the excited

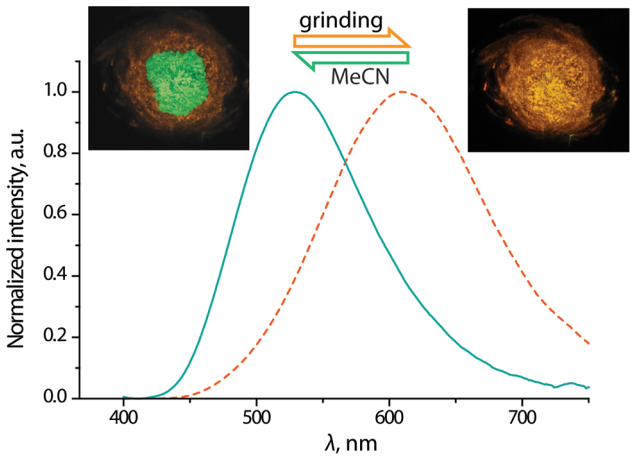

Figure 8. Spectroscopic changes of complex **10** (all forms) upon grinding and treatment with acetonitrile.

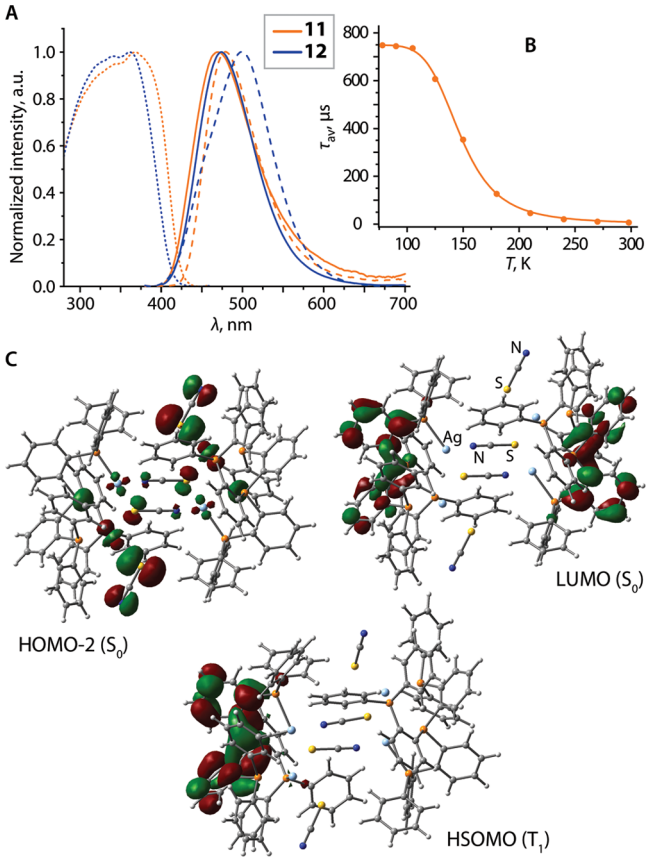

Figure 9. (A) Normalized solid-state excitation (dotted lines, 298 K) and emission spectra (solid lines, 298 K; dashed lines, 77 K) of **11** and **12**. (B) Temperature dependence of average lifetimes of **11** (the solid line is the fit according to eq 1). (C) Selected frontier orbitals in the ground state (S_0) and the highest singly occupied molecular orbital of the lowest excited triplet state (T_1) of **11** (optimized geometries).

states (Table S9), also has a visibly longer lifetime at 77 K (τ_{obs} = 748 μs for **11**, 220 μs for **12**) likely as a consequence of a weaker spin−orbit coupling due to less explicit metallophilic interactions. The highest occupied MOs for **11** are mainly localized on terminal thiocyanate ligands (Figure 9 and Figure S16), which therefore have a crucial effect on the electronic structures of these clusters. The lowest allowed electronic excitation, which is $S_0 \rightarrow S_2$ for both **11** and **12** (Table S7), in the case of **11** involves HOMO − 2/HOMO − 3 → LUMO/LUMO + 1 transitions and has a clear L′LCT (t-SCN → $\pi\mathbf{P}^3$) character with some MLCT (metal atoms contribute 16%/18% to HOMO − 3/HOMO − 2, Table S8) and L″LCT (μ-SCN → $\pi\mathbf{P}^3$) admixtures.

In **12**, the HOMO and HOMO − 1 are distributed over the silver ions and phosphorus atoms with SCN bridges only constituting 6% and 4%, respectively. This allows us to ascribe the predicted $S_0 \rightarrow S_2$ excitation to the (d,p(Ag, P) → $\pi\mathbf{P}^3$) charge transfer parentage, analogously to its cyanide relative $[Ag_2(\mu_2\text{-CN})(\mathbf{P^4})]_2^{2+}$.[50] However, in **11** and **12** the frontier orbitals are distributed asymmetrically in the lowest lying triplet state (Figure 9 and Figure S16); the latter can be described essentially in the same terms as the forgoing singlet−singlet excitations, i.e., having ^{3}(L′ + M)LCT (**11**) and ^{3}(L + M)LCT (**12**) origins.

The emission of cluster **17** (λ_{em} = 470 nm), which is formally derived from **12** by changing the triflate counterion to

DOI: 10.1021/acs.inorgchem.8b03166
Inorg. Chem. 2019, 58, 3646−3660

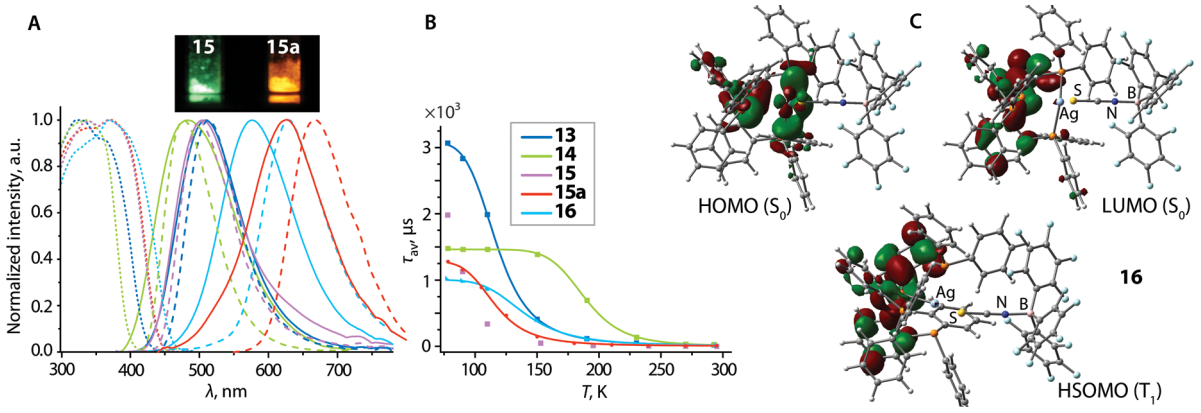

Figure 10. (A) Normalized solid-state excitation (dotted lines, 298 K) and emission spectra (solid lines, 298 K; dashed lines, 77 K) of **13**–**16** (the photograph shows the appearance of **15** and **15a** under UV light at 298 K). (B) Temperature dependencies of average lifetimes of **13**–**16** (the solid lines are the fits according to eq 1). (C) Frontier orbitals in the ground state (S_0) and the highest singly occupied molecular orbital of the lowest excited triplet state (T_1) of complex **16** (optimized geometries).

$[SCN:B(C_6F_5)_3]^-$, is very close to those of **11** and **12**, although the intensity is decreased to 4%. Because the nonradiative rate constant for **17** is comparable to those for **11** and **12** (see Table 1), the drop of the quantum yield corresponds to the slowdown of the radiative relaxation (k_r = 6.3 × 10^3 s^{-1} for **17** vs 3.1 × 10^4 s^{-1} for **12**), presumably caused by the differences in the ligand sphere (**17**, in contrast to **12**, contains coordinated THF molecules, Figure S5).

The borane-containing complexes **13**–**15** (except form **15a**) reveal blue-shifted luminescence (λ_{em} = 505–482 nm, Figure 10 and Table 1) with respect to that of their parent compounds **7**–**9** (λ_{em} = 520–543 nm). Remarkably, the THF-solvated form of **15** shows blue-greenish emission (λ_{em} = 505 nm), but the solvent-free crystalline modification emits in the orange region (λ_{em} = 625 nm, Figure 10), which is quite close to its behavior in THF solution (λ_{em} = 650 nm, Φ_{em} = 2.1%). On the other hand, in the case of **16** we were able to obtain only one crystalline form (λ_{em} = 575 nm) in contrast to its versatile congener **10**. The relaxed geometries of tetraphosphine species **15** and **16** in the S_1 and T_1 states (the optimization of S_1 state could not be achieved for **16**) reveal the same sort of structural changes as theoretically predicted for **9** and **10**, leading to the contraction of the longest nonbonding P···metal distance and emergence of the pentacoordinate coordination environment of the metal ions (Figure S17).

The addition of the $B(C_6F_5)_3$ groups resulted in a ca. 4- to 6-fold decrease of radiative rate constants in **13**–**16** vs **7**–**10** that consequently increased the observed lifetimes (both at 298 and 77 K) and lowered quantum efficiency, particularly for the silver compounds **14** and **16**. The phosphorescence decay times $\tau(T_1)$ for **13**–**16** are systematically longer than for their corresponding precursors **7**–**10** and reach the value of 3 ms (Table 2), denoting rather weak SOC that can be attributed to the change of the electronic structures upon boronation. The calculated S_1 state for **13**–**16** results from a nearly pure HOMO → LUMO transition, which has a d,p(M, P) → $\pi P^{3/4}$ character, the opposite of **7**–**10**, with a very small (1–2%) contribution of $SCN:B(C_6F_5)_3$ ligand, i.e., the excited states S_1 and T_1 for **13**–**16** can be classified as (L + M)LCT, see Figure 10 and Figure S18.

CONCLUSIONS

The family of thiocyanate copper(I) and silver(I) compounds was prepared using the series of chelating bi-, tri-, and tetraphosphines. The denticity of P-donor ligands and the potentially bridging coordinating ability of SCN groups determines the nuclearity of the resulting products, which comprise mono-, di-, and tetrametallic species. The dinuclear complexes, containing diphosphines DPEphos, Xantphos, and dppb, in the solid state feature the $M\binom{SCN}{NCS}M$ metallacycles as the preferential structural motif (**1**, **3**–**6**). The only exception is the disilver compound **2**, having the sulfur-bridged metal ions. The ambidentate character of the thiocyanate is also realized in the mononuclear complexes **7**–**10**, which reveal the N-coordination mode for the copper compounds and predominantly S-coordination for their silver congeners. The tetraphosphine silver complex **10** can be converted into the tetrametallic aggregates by reacting with an equimolar amount of silver salts AgSCN (**11**) or $AgCF_3SO_3$ (**12**). In addition, treatment of **7**–**11** with strong Lewis acid $B(C_6F_5)_3$ leads to their isothiocyanatoborate derivatives **13**–**17**, which bear weakly coordinating $^-SCN:B(C_6F_5)_3$ ligand.

The luminescence properties of compounds **1** and **5**–**17** were investigated in the solid state; the dinuclear species **2**–**4** did not show appreciable emission under ambient conditions. The studied complexes demonstrate delayed fluorescence at room temperature. The calculated electronic structures suggest the charge transfer character of the S_1 and T_1 excited states. In particular, the lowest energy electronic transitions in **7**–**11**, having terminally coordinated SCN ligands, are mainly of L′LCT SCN → π(phosphine) origin (except **10**) with some contribution of the MLCT process due to localization of the HOMO and LUMO on the thiocyanate and phosphine's aromatic groups, respectively. The bridging bonding of SCN decreases its contribution to the highest occupied orbitals in **1**, **5**, **6**, and **12**, thus increasing the role of d,p(M, P) → π(phosphine) transitions in the formation of the excited states. For **13**–**16**, this effect is even more pronounced as the boronation of the N-donor nearly completely switches off the SCN → π charge transfer that changes the nature of S_1 and T_1 states to (L + M)LCT (d,p(M, P) → $\pi P^{3/4}$).

Because the characteristics of excited states are mainly governed by the phosphine ligands and their coordination

DOI: 10.1021/acs.inorgchem.8b03166
Inorg. Chem. 2019, 58, 3646–3660

mode, a wide variation of the emission energies has been achieved and covers the range from blue (λ_{em} = 448 nm, **1**) to red-orange (λ_{em} = 630 nm, **10c**). Interestingly, the luminescence color for the tetraphosphine complexes **10** and **15**, which were obtained in several forms, is strongly dependent on the crystal packing and shows dramatic alteration for **15** (λ_{em} = 505 and 625 nm). This phenomenon has been tentatively assigned to the significant geometry reorganizations that occur in both S_1 and T_1 excited states for the complexes with S-coordinated SCN/SCN:B$(C_6F_5)_3$ ligands. The predicted distortions, which involve the contraction of nonbonding P···M separation for ca. 1.5 Å and the formation of the 5-coordinate coordination environment of the d^{10} metals, might be substantially confined by the lattice and thus influence the energy of the emissive S_1 state. Such a molecular design, which allows severe photoinduced deformations, opens a simple though effective approach to the versatile TADF d^{10} complexes, e.g., exhibiting stimuli-responsive emission.

■ ASSOCIATED CONTENT

Supporting Information

The Supporting Information is available free of charge on the ACS Publications website at DOI: 10.1021/acs.inorgchem.8b03166.

Crystallographic and computational details; molecular views of selected complexes; ESI-MS, NMR, and additional photophysical data; and electron density plots (PDF)

Accession Codes

CCDC 1878279−1878303 contain the supplementary crystallographic data for this paper. These data can be obtained free of charge via www.ccdc.cam.ac.uk/data_request/cif, or by emailing data_request@ccdc.cam.ac.uk, or by contacting The Cambridge Crystallographic Data Centre, 12 Union Road, Cambridge CB2 1EZ, UK; fax: +44 1223 336033.

■ AUTHOR INFORMATION

Corresponding Author

*E-mail: igor.koshevoy@uef.fi. (I.O.K.)

ORCID

Igor O. Koshevoy: 0000-0003-4380-1302

Present Address

[‖]Turku University, Department of Chemistry, Vatselankatu 2, 20014 Turku, Finland (C.D.).

Notes

The authors declare no competing financial interest.

■ ACKNOWLEDGMENTS

The authors appreciate the financial support from the Russian Science Foundation (grant 16-13-10064, E.V.G., photophysical studies) and the Academy of Finland (grant 317903, I.O.K.). We acknowledge grants of computer capacity from the Finnish Grid and Cloud Infrastructure (persistent identifier urn:nbn:fi:research-infras-2016072533). The work was carried out using the core facilities of St. Petersburg State University Research Park (Centre for Magnetic Resonance, Centre for Optical and Laser Materials Research), and the Analytical Centre for Nano- and Biotechnologies (Peter the Great St. Petersburg Polytechnic University, with financial support from Ministry of Education and Science of Russian Federation).

■ REFERENCES

(1) Czerwieniec, R.; Leitl, M. J.; Homeier, H. H. H.; Yersin, H. Cu(I) complexes − Thermally activated delayed fluorescence. Photophysical approach and material design. *Coord. Chem. Rev.* **2016**, *325*, 2−28.

(2) Ohara, H.; Kobayashi, A.; Kato, M. Simple and extremely efficient blue emitters based on mononuclear Cu(I)-halide complexes with delayed fluorescence. *Dalton Trans.* **2014**, *43*, 17317−17323.

(3) Nitsch, J.; Lacemon, F.; Lorbach, A.; Eichhorn, A.; Cisnetti, F.; Steffen, A. Cuprophilic interactions in highly luminescent dicopper(I)−NHC−picolyl complexes − fast phosphorescence or TADF? *Chem. Commun.* **2016**, *52*, 2932−2935.

(4) Li, G.; Nobuyasu, R. S.; Zhang, B.; Geng, Y.; Yao, B.; Xie, Z.; Zhu, D.; Shan, G.; Che, W.; Yan, L.; Su, Z.; Dias, F. B.; Bryce, M. R. Thermally Activated Delayed Fluorescence in CuI Complexes Originating from Restricted Molecular Vibrations. *Chem. - Eur. J.* **2017**, *23*, 11761−11766.

(5) Hofbeck, T.; Monkowius, U.; Yersin, H. Highly Efficient Luminescence of Cu(I) Compounds: Thermally Activated Delayed Fluorescence Combined with Short-Lived Phosphorescence. *J. Am. Chem. Soc.* **2015**, *137*, 399−404.

(6) Osawa, M.; Kawata, I.; Ishii, R.; Igawa, S.; Hashimoto, M.; Hoshino, M. Application of neutral d^{10} coinage metal complexes with an anionic bidentate ligand in delayed fluorescence-type organic light-emitting diodes. *J. Mater. Chem. C* **2013**, *1*, 4375−4383.

(7) Volz, D.; Chen, Y.; Wallesch, M.; Liu, R.; Fléchon, C.; Zink, D. M.; Friedrichs, J.; Flügge, H.; Steininger, R.; Göttlicher, J.; Heske, C.; Weinhardt, L.; Bräse, S.; So, F.; Baumann, T. Bridging the Efficiency Gap: Fully Bridged Dinuclear Cu(I)-Complexes for Singlet Harvesting in High-Efficiency OLEDs. *Adv. Mater.* **2015**, *27*, 2538−2543.

(8) Osawa, M.; Hoshino, M.; Hashimoto, M.; Kawata, I.; Igawa, S.; Yashima, M. Application of three-coordinate copper(I) complexes with halide ligands in organic light-emitting diodes that exhibit delayed fluorescence. *Dalton Trans.* **2015**, *44*, 8369−8378.

(9) Liang, D.; Chen, X.-L.; Liao, J.-Z.; Hu, J.-Y.; Jia, J.-H.; Lu, C.-Z. Highly Efficient Cuprous Complexes with Thermally Activated Delayed Fluorescence for Solution-Processed Organic Light-Emitting Devices. *Inorg. Chem.* **2016**, *55*, 7467−7475.

(10) Zhang, F.; Guan, Y.; Chen, X.; Wang, S.; Liang, D.; Feng, Y.; Chen, S.; Li, S.; Li, Z.; Zhang, F.; Lu, C.; Cao, G.; Zhai, B. Syntheses, Photoluminescence, and Electroluminescence of a Series of Sublimable Bipolar Cationic Cuprous Complexes with Thermally Activated Delayed Fluorescence. *Inorg. Chem.* **2017**, *56*, 3742−3753.

(11) Xie, M.; Han, C.; Zhang, J.; Xie, G.; Xu, H. White Electroluminescent Phosphine-Chelated Copper Iodide Nanoclusters. *Chem. Mater.* **2017**, *29*, 6606−6610.

(12) Bizzarri, C.; Hundemer, F.; Busch, J.; Bräse, S. Triplet emitters versus TADF emitters in OLEDs: A comparative study. *Polyhedron* **2018**, *140*, 51−66.

(13) Zink, D. M.; Volz, D.; Baumann, T.; Mydlak, M.; Flugge, H.; Friedrichs, J.; Nieger, M.; Brase, S. Heteroleptic, Dinuclear Copper(I) Complexes for Application in Organic Light-Emitting Diodes. *Chem. Mater.* **2013**, *25*, 4471−4448.

(14) Wallesch, M.; Volz, D.; Zink, D. M.; Schepers, U.; Nieger, M.; Baumann, T.; Brase, S. Bright Coppertunities: Multinuclear CuI Complexes with N−P Ligands and Their Applications. *Chem. - Eur. J.* **2014**, *20*, 6578−6590.

(15) Musina, E. I.; Shamsieva, A. V.; Strelnik, I. D.; Gerasimova, T. P.; Krivolapov, D. B.; Kolesnikov, I. E.; Grachova, E. V.; Tunik, S. P.; Bannwarth, C.; Grimme, S.; Katsyuba, S. A.; Karasik, A. A.; Sinyashin, O. G. Synthesis of novel pyridyl containing phospholanes and their polynuclear luminescent copper(I) complexes. *Dalton Trans.* **2016**, *45*, 2250−2260.

(16) Okano, Y.; Ohara, H.; Kobayashi, A.; Yoshida, M.; Kato, M. Systematic Introduction of Aromatic Rings to Diphosphine Ligands for Emission Color Tuning of Dinuclear Copper(I) Iodide Complexes. *Inorg. Chem.* **2016**, *55*, 5227−5236.

(17) Ohara, H.; Ogawa, T.; Yoshida, M.; Kobayashi, A.; Kato, M. Reversible luminescent colour changes of mononuclear copper(i)

DOI: 10.1021/acs.inorgchem.8b03166
Inorg. Chem. 2019, 58, 3646−3660

complexes based on ligand exchange reactions by N-heteroaromatic vapours. *Dalton Trans.* **2017**, *46*, 3755−3760.
(18) Zeng, C.; Wang, N.; Peng, T.; Wang, S. Copper(I) Complexes Bearing 1,2-Phenyl-Bridged P∧N, P∧N∧P, and N∧P∧N Chelate Ligands: Structures and Phosphorescence. *Inorg. Chem.* **2017**, *56*, 1616−1625.
(19) Hupp, B.; Schiller, C.; Lenczyk, C.; Stanoppi, M.; Edkins, K.; Lorbach, A.; Steffen, A. Synthesis, Structures, and Photophysical Properties of a Series of Rare Near-IR Emitting Copper(I) Complexes. *Inorg. Chem.* **2017**, *56*, 8996−9008.
(20) Chen, J.; Teng, T.; Kang, L.; Chen, X.-L.; Wu, X.-Y.; Yu, R.; Lu, C.-Z. Highly Efficient Thermally Activated Delayed Fluorescence in Dinuclear Ag(I) Complexes with a Bis-Bidentate Tetraphosphane Bridging Ligand. *Inorg. Chem.* **2016**, *55*, 9528−9536.
(21) Shafikov, M. Z.; Suleymanova, A. F.; Czerwieniec, R.; Yersin, H. Thermally Activated Delayed Fluorescence from Ag(I) Complexes: A Route to 100% Quantum Yield at Unprecedentedly Short Decay Time. *Inorg. Chem.* **2017**, *56*, 13274−13285.
(22) Gan, X.-M.; Yu, R.; Chen, X.-L.; Yang, M.; Lin, L.; Wu, X.-Y.; Lu, C.-Z. A unique tetranuclear Ag(i) complex emitting efficient thermally activated delayed fluorescence with a remarkably short decay time. *Dalton Trans.* **2018**, *47*, 5956−5960.
(23) Shafikov, M. Z.; Suleymanova, A. F.; Schinabeck, A.; Yersin, H. Dinuclear Ag(I) Complex Designed for Highly Efficient Thermally Activated Delayed Fluorescence. *J. Phys. Chem. Lett.* **2018**, *9*, 702−709.
(24) Osawa, M.; Hashimoto, M.; Kawata, I.; Hoshino, M. Photoluminescence properties of TADF-emitting three-coordinate silver(i) halide complexes with diphosphine ligands: a comparison study with copper(i) complexes. *Dalton Trans.* **2017**, *46*, 12446−12455.
(25) Chakkaradhari, G.; Chen, Y.-T.; Karttunen, A. J.; Dau, M. T.; Jänis, J.; Tunik, S. P.; Chou, P.-T.; Ho, M.-L.; Koshevoy, I. O. Luminescent Triphosphine-Cyanide d^{10} Metal Complexes. *Inorg. Chem.* **2016**, *55*, 2174−2184.
(26) Belyaev, A.; Dau, T. M.; Jänis, J.; Grachova, E. V.; Tunik, S. P.; Koshevoy, I. O. Low-Nuclearity Alkynyl d^{10} Clusters Supported by Chelating Multidentate Phosphines. *Organometallics* **2016**, *35*, 3763−3774.
(27) *APEX2—Software Suite for Crystallographic Programs*; Bruker AXS, Inc.: Madison, WI, 2010.
(28) Sheldrick, G. M. Crystal structure refinement with SHELXL. *Acta Crystallogr., Sect. C: Struct. Chem.* **2015**, *71*, 3−8.
(29) Farrugia, L. J. WinGX and ORTEP for Windows: an Update. *J. Appl. Crystallogr.* **2012**, *45*, 849−854.
(30) Sheldrick, G. M. *SADABS-2008/1—Bruker AXS Area Detector Scaling and Absorption Correction*; Bruker AXS: Madison, WI, 2008.
(31) Spek, A. L. PLATON SQUEEZE: a tool for the calculation of the disordered solvent contribution to the calculated structure factors. *Acta Crystallogr., Sect. C: Struct. Chem.* **2015**, *C71*, 9−18.
(32) Spek, A. L. *PLATON, A Multipurpose Crystallographic Tool, 1.17*; Utrecht University: Utrecht, The Netherlands, 2013.
(33) Brouwer, A. M. Standards for photoluminescence quantum yield measurements in solution (IUPAC Technical Report). *Pure Appl. Chem.* **2011**, *83*, 2213−2228.
(34) Frisch, M. J.; Trucks, G. W.; Schlegel, H. B.; Scuseria, G. E.; Robb, M. A.; Cheeseman, J. R.; Scalmani, G.; Barone, V.; Petersson, G. A.; Nakatsuji, H.; Li, X.; Caricato, M.; Marenich, A. V.; Bloino, J.; Janesko, B. G.; Gomperts, R.; Mennucci, B.; Hratchian, H. P.; Ortiz, J. V.; Izmaylov, A. F.; Sonnenberg, J. L.; Williams-Young, D.; Ding, F.; Lipparini, F.; Egidi, F.; Goings, J.; Peng, B.; Petrone, A.; Henderson, T.; Ranasinghe, D.; Zakrzewski, V. G.; Gao, J.; Rega, N.; Zheng, G.; Liang, W.; Hada, M.; Ehara, M.; Toyota, K.; Fukuda, R.; Hasegawa, J.; Ishida, M.; Nakajima, T.; Honda, Y.; Kitao, O.; Nakai, H.; Vreven, T.; Throssell, K.; Montgomery, J. A. J.; Peralta, J. E.; Ogliaro, F.; Bearpark, M. J.; Heyd, J. J.; Brothers, E. N.; Kudin, K. N.; Staroverov, V. N.; Keith, T. A.; Kobayashi, R.; Normand, J.; Raghavachari, K.; Rendell, A. P.; Burant, J. C.; Iyengar, S. S.; Tomasi, J.; Cossi, M.; Millam, J. M.; Klene, M.; Adamo, C.; Cammi, R.; Ochterski, J. W.; Martin, R. L.; Morokuma, K.; Farkas, O.; Foresman, J. B.; Fox, D. J. *Gaussian 16*; Gaussian, Inc.: Wallingford CT, 2016.
(35) Perdew, J. P.; Burke, K.; Ernzerhof, M. Generalized Gradient Approximation Made Simple. *Phys. Rev. Lett.* **1996**, *77*, 3865−3868.
(36) Adamo, C.; Barone, V. Toward reliable density functional methods without adjustable parameters: The PBE0 model. *J. Chem. Phys.* **1999**, *110*, 6158−6170.
(37) Rappoport, D.; Furche, F. Property-optimized Gaussian basis sets for molecular response calculations. *J. Chem. Phys.* **2010**, *133*, 134105.
(38) Trivedi, M.; Ujjain, S. K.; Singh, G.; Kumar, A.; Dubey, S. K.; Rath, N. P. Syntheses, characterization, and electrochemistry of compounds containing 1-diphenylphosphino-10-(di-tert-butylphosphino)ferrocene (dppdtbpf). *J. Organomet. Chem.* **2014**, *772*−*773*, 202−209.
(39) Bowmaker, G. A.; Hanna, J. V.; King, S. P.; Marchetti, F.; Pettinari, C.; Pizzabiocca, A.; Skelton, B. W.; Sobolev, A. N.; Tăbăcaru, A.; White, A. H. Complexes of Copper(I) Thiocyanate with Monodentate Phosphine and Pyridine Ligands and the P(,N)-Donor Diphenyl(2-pyridyl)phosphine. *Eur. J. Inorg. Chem.* **2014**, *2014*, 6104−6116.
(40) Cingolani, A.; Di Nicola, C.; Effendy; Pettinari, C.; Skelton, B. W.; Somers, N.; White, A. H. New oligo-/poly-meric forms for MX:dpex (1:1) complexes (M = CuI, AgI; X = (pseudo-)halide; dpex = $Ph_2E(CH_2)_xEPh_2$, E = (P), As; x = 1, 2). *Inorg. Chim. Acta* **2005**, *358*, 748−762.
(41) Bowmaker, G. A.; Hanna, J. V.; Hart, R. D.; Healy, P. C.; King, S. P.; Marchetti, F.; Pettinari, C.; Skelton, B. W.; Tabacaru, A.; White, A. H. Mechanochemical and solution synthesis, X-ray structure and IR and 31P solid state NMR spectroscopic studies of copper(i) thiocyanate adducts with bulky monodentate tertiary phosphine ligands. *Dalton Trans.* **2012**, *41*, 7513−7525.
(42) Bowmaker, G. A.; Di Nicola, C.; Effendy; Hanna, J. V.; Healy, P. C.; King, S. P.; Marchetti, F.; Pettinari, C.; Robinson, W. T.; Skelton, B. W.; Sobolev, A. N.; Tăbăcaru, A.; White, A. H. Oligonuclear silver thiocyanate complexes with monodentate tertiary phosphine ligands, including novel 'cubane' and 'step' tetramer forms of AgSCN: PR_3 $(1:1)_4$. *Dalton Trans.* **2013**, *42*, 277−291.
(43) Škoch, K.; Uhlík, F.; Císařová, I.; Štěpnička, P. Silver(i) complexes with 1′-(diphenylphosphino)-1-cyanoferrocene: the art of improvisation in coordination. *Dalton Trans.* **2016**, *45*, 10655−10671.
(44) Artem'ev, A. V.; Ryzhikov, M. R.; Taidakov, I. V.; Rakhmanova, M. I.; Varaksina, E. A.; Bagryanskaya, I. Y.; Malysheva, S. F.; Belogorlova, N. A. Bright green-to-yellow emitting Cu(i) complexes based on bis(2-pyridyl)phosphine oxides: synthesis, structure and effective thermally activated-delayed fluorescence. *Dalton Trans.* **2018**, *47*, 2701−2710.
(45) Jia, J.-H.; Kang, L.-J.; Yu, R.-M.; Lu, C.-Z. Synthesis, Crystal Structure and Photoluminescence of a Dinuclear Cuprous Complex with Thiocyanate Bridges. *Chin. J. Struct. Chem.* **2016**, *35*, 1593−1599.
(46) Di Nicola, C.; Effendy; Pettinari, C.; Skelton, B. W.; Somers, N.; White, A. H. The structural definition of adducts of stoichiometry AgX:dppf $(1:1_{)(n)}$, X = simple anion, dppf = bis(diphenylphosphino)-ferrocene. *Inorg. Chim. Acta* **2005**, *358*, 695−706.
(47) Omondi, B.; Venter, G. J. S.; Roodt, A.; Meijboom, R. Isomorphism in monomeric 1:3 complexes of silver(I) salts with tri-p-tolylphosphine. *Acta Crystallogr., Sect. B: Struct. Sci.* **2009**, *B65*, 699−706.
(48) Zank, J.; Schier, A.; Schmidbaur, H. Gold and silver cations in the ″Procrustean Bed″ of the bis[2-(diphenylphosphino)phenyl]-phenylphosphine ligand. Observations and conclusions. *J. Chem. Soc., Dalton Trans.* **1999**, 415−420.
(49) Dau, T. M.; Asamoah, B. D.; Belyaev, A.; Chakkaradhari, G.; Hirva, P.; Jänis, J.; Grachova, E. V.; Tunik, S. P.; Koshevoy, I. O. Adjustable coordination of a hybrid phosphine-phosphine oxide ligand in luminescent Cu, Ag and Au complexes. *Dalton Trans.* **2016**, *45*, 14160−14173.

DOI: 10.1021/acs.inorgchem.8b03166
Inorg. Chem. 2019, 58, 3646−3660

(50) Belyaev, A.; Eskelinen, T.; Dau, T. M.; Ershova, Y. Y.; Tunik, S. P.; Melnikov, A. S.; Hirva, P.; Koshevoy, I. O. Cyanide-assembled d^{10} coordination polymers and cycles: excited state metallophilic modulation of solid-state luminescence. *Chem. - Eur. J.* **2018**, *24*, 1404−1415.
(51) Chu, W.-K.; Wei, X.-G.; Yiu, S.-M.; Ko, C.-C.; Lau, K.-C. Strongly Phosphorescent Neutral Rhenium(I) Isocyanoborato Complexes: Synthesis, Characterization, and Photophysical, Electrochemical, and Computational Studies. *Chem. - Eur. J.* **2015**, *21*, 2603−2612.
(52) Chan, K.-C.; Chu, W.-K.; Yiu, S.-M.; Ko, C.-C. Synthesis, characterization, photophysics and electrochemical study of luminescent iridium(III) complexes with isocyanoborate ligands. *Dalton Trans.* **2015**, *44*, 15135−15144.
(53) Chan, K.-C.; Cheng, S.-C.; Lo, L. T.-L.; Yiu, S.-M.; Ko, C.-C. Luminescent Charge-Neutral Copper(I) Phenanthroline Complexes with Isocyanoborate Ligand. *Eur. J. Inorg. Chem.* **2018**, *2018*, 897−903.
(54) Pearson, R. G. Hard and Soft Acids and Bases. *J. Am. Chem. Soc.* **1963**, *85*, 3533−3539.
(55) Munro, O. Q.; Pearson, N. The isothiocyanate complex of triphenylborane forms an unusual coordination polymer with $[K(18\text{-crown-}6)]^+$, both in the solid state and in solution. *Acta Crystallogr., Sect. C: Cryst. Struct. Commun.* **2003**, *C59*, m407−m412.
(56) Vei, I. C.; Pascu, S. I.; Green, M. L. H.; Green, J. C.; Schilling, R. E.; Anderson, G. D. W.; Rees, L. H. Synthesis and study of new binuclear compounds containing bridging $(\mu\text{-CN})B(C_6F_5)_3$ and $(\mu\text{-NC})B(C_6F_5)_3$ systems. *Dalton Trans.* **2003**, 2550−2557.
(57) Doux, M.; Ricard, L.; Le Floch, P.; Mézailles, N. Group 11 metal complexes of SPS-based pincer ligands: Syntheses, X-ray structures and reactivity. *Dalton Trans.* **2004**, 2593−2600.
(58) Jarvis, A. G.; Whitwood, A. C.; Fairlamb, I. J. S. CuI complexes containing a multidentate and conformationally flexible dibenzylidene acetone ligand (dbathiophos): Application in catalytic alkene cyclopropanation. *Dalton Trans.* **2011**, *40*, 3695−3702.
(59) Tsukuda, T.; Miyoshi, R.; Esumi, A.; Yamagiwa, A.; Dairiki, A.; Matsumoto, K.; Tsubomura, T. Sulfur transfer reaction from phosphine sulfides to phosphines assisted by metal ions. *Inorg. Chim. Acta* **2012**, *384*, 149−153.
(60) Wang, Y.; Cui, Y.-Z.; Liu, M.; Wang, M.-Q.; Geng, W.-X.; Li, Z.-F.; Jin, Q.-H. Syntheses, Characterization and Luminescent Properties of Silver(I) Complexes Based on Diphosphine Ligands. *Chin. J. Inorg. Chem.* **2018**, *34*, 381−386.
(61) Osawa, M. Highly efficient blue-green delayed fluorescence from copper(I) thiolate complexes: luminescence color alteration by orientation change of the aryl ring. *Chem. Commun.* **2014**, *50*, 1801−1803.
(62) Chen, J.; Teng, T.; Wang, J.-Y.; Kang, L.; Chen, X.-L.; Xu, L.-J.; Yu, R.; Lu, C.-Z. Synthesis, Structure, and Characterization of Emissive Neutral Dinuclear CuI Complexes with a Tetraphosphane Bridging Ligand. *Eur. J. Inorg. Chem.* **2016**, *2016*, 3036−3041.
(63) Coppens, P.; Sokolow, J.; Trzop, E.; Makal, A.; Chen, Y. On the Biexponential Decay of the Photoluminescence of the Two Crystallographically-Independent Molecules in Crystals of $[Cu(I)(phen)(PPh_3)_2][BF_4]$. *J. Phys. Chem. Lett.* **2013**, *4*, 579−582.
(64) Turro, N. J.; Ramamurthy, V.; Scaiano, J. C. *Modern Molecular Photochemistry of Organic Molecules*; University Science Books: Sausalito, CA, 2010.

DOI: 10.1021/acs.inorgchem.8b03166
Inorg. Chem. 2019, 58, 3646−3660